



Available online at www.sciencedirect.com

ScienceDirect

Comput. Methods Appl. Mech. Engrg. 396 (2022) 115104

Computer methods in applied mechanics and engineering

www.elsevier.com/locate/cma

Efficient optimization-based quadrature for variational discretization of nonlocal problems

Marco Pasetto^{a,*}, Zhaoxiang Shen^b, Marta D'Elia^c, Xiaochuan Tian^d, Nathaniel Trask^e, David Kamensky^a

^a Department of Mechanical and Aerospace Engineering, University of California, San Diego, La Jolla, CA 92093, USA

^b Department of Engineering, Faculty of Science, Technology and Medicine, University of Luxembourg, Esch-sur-Alzette 4365, Luxembourg

- ^c Data Science and Computing, Sandia National Laboratories, Livermore, CA 94550, USA
- ^d Department of Mathematics, University of California, San Diego, La Jolla, CA 92093, USA
- ^e Center for Computing Research, Sandia National Laboratories, Albuquerque, NM 87185, USA

Received 25 January 2022; received in revised form 25 April 2022; accepted 2 May 2022 Available online 23 May 2022

Abstract

Casting nonlocal problems in variational form and discretizing them with the finite element (FE) method facilitates the use of nonlocal vector calculus to prove well-posedness, convergence, and stability of such schemes. Employing an FE method also facilitates meshing of complicated domain geometries and coupling with FE methods for local problems. However, nonlocal weak problems involve the computation of a double-integral, which is computationally expensive and presents several challenges. In particular, the inner integral of the variational form associated with the stiffness matrix is defined over the intersections of FE mesh elements with a ball of radius δ , where δ is the range of nonlocal interaction. Identifying and parameterizing these intersections is a nontrivial computational geometry problem. In this work, we propose a quadrature technique where the inner integration is performed using quadrature points distributed over the full ball, without regard for how it intersects elements, and weights are computed based on the generalized moving least squares method. Thus, as opposed to all previously employed methods, our technique does not require element-by-element integration and fully circumvents the computation of element-ball intersections. This paper considers one- and two-dimensional implementations of piecewise linear continuous FE approximations, focusing on the case where the element size h and the nonlocal radius δ are proportional, as is typical of practical computations. When boundary conditions are treated carefully and the outer integral of the variational form is computed accurately, the proposed method is asymptotically compatible in the limit of $h \sim \delta \to 0$, featuring at least first-order convergence in L^2 for all dimensions, using both uniform and nonuniform grids. Moreover, in the case of uniform grids, the proposed method passes a patch test and, according to numerical evidence, exhibits an optimal, second-order convergence rate. Our numerical tests also indicate that, even for nonuniform grids, second-order convergence can be observed over a substantial pre-asymptotic regime.

© 2022 Elsevier B.V. All rights reserved.

Keywords: Nonlocal models; Finite element discretizations; Generalized moving least squares; Numerical quadrature; Peridynamics

E-mail address: mpasetto@ucsd.edu (M. Pasetto).

^{*} Corresponding author.

1. Introduction

Nonlocal models have become viable alternatives to partial differential equations (PDEs) for applications where small-scale effects affect the global behavior of a system or when discontinuities in the quantity of interest make it impractical to use differential operators. In fact, nonlocal operators embed length scales in their definitions and allow for irregular functions. For these reasons, nonlocal models are currently employed in several scientific and engineering applications including surface or subsurface transport [1–6], fracture mechanics [7–9], turbulence [10–12], image processing [13–15] and stochastic processes [16–20].

Nonlocal operators are integral operators that embed length scales in the domain of integration; as such, they allow one to model long-range forces within the length scale and to reduce the regularity requirements on the solutions. The most general form of nonlocal Laplace operator is given by [21]

$$\mathcal{L}_{\delta}u(\mathbf{x}) = 2 \int_{\mathbb{R}^n} (u(\mathbf{y}) - u(\mathbf{x})) \gamma(\mathbf{x}, \mathbf{y}) \, d\mathbf{y},$$

where $u: \mathbb{R}^n \to \mathbb{R}$ is a scalar function and γ is a symmetric *kernel* function whose support is $\mathcal{H}(\mathbf{x}, \delta)$, the ball centered at \mathbf{x} of radius δ , the so-called horizon or interaction radius. In most cases, the ball is understood in the Euclidean sense (to maintain rotational invariance), but recent works also employ more general balls, including ℓ^{∞} balls, see, e.g. [22–24]. The function γ determines the function space that the nonlocal solution belongs to. Its choice is nontrivial and non-intuitive; in fact, the selection of the optimal kernel is a widely studied research question [12,25–34].

Because of the integral nature of nonlocal operators, the discretization and numerical solution of nonlocal equations raises several unresolved challenges. These include the design of accurate and efficient discretization schemes and the development of efficient numerical solvers [35–42]. With the ultimate goal of easily handling nontrivial domains and possibly using mesh adaptivity, this work focuses on variational discretizations and, specifically, the finite element method. However, we point out that the nonlocal literature offers a broad class of meshfree techniques, widely used at the engineering level. We refer the interested reader to, e.g., [40,41,43–46]. One advantage of the FE method is that the nonlocal vector calculus facilitates its numerical analysis. This theoretical framework, first introduced in [47], further developed in [48], and generalized in [21], allows us to cast nonlocal equations in a variational setting and analyze them in the same way as PDEs. Using this framework, one can prove well-posedness, convergence, and stability of nonlocal FE schemes. Nonetheless, variational discretizations introduce further computational challenges due to the presence of an additional integration over the domain of the problem. In fact, the nonlocal weak problem associated with the operator \mathcal{L}_{δ} involves the computation of a double integral. Specifically, the core computation required by standard codes to assemble the FE stiffness matrix is given by an integral of the form

$$\int_{\Omega_i^h} \int_{\Omega_i^h \cap \mathcal{H}(\mathbf{x},\delta)} [\psi_k(\mathbf{y}) - \psi_k(\mathbf{x})] \gamma(\mathbf{x},\mathbf{y}) [\psi_l(\mathbf{y}) - \psi_l(\mathbf{x})] \, d\mathbf{y} \, d\mathbf{x},\tag{1}$$

where Ω_i^h is the *i*th element of the partition and ψ_k is the *k*th FE basis function. (See Section 4 for a complete formulation.) In the formula above, we have purposely written the inner domain of integration explicitly, to highlight the fact that, prior to numerically evaluating the integral, we must identify the region of the *j*th element that overlaps with the support of the kernel function, since a naïve, global integration over the whole element would not guarantee numerical convergence of the overall scheme. Identifying this region is a nontrivial, time-consuming task. Furthermore, the presence of a double integral inevitably adds computational cost and it is often the case that the integrand function is singular, requiring the use of sophisticated, possibly adaptive quadrature rules.

A thorough description of the computational challenges that arise in the computation of the double integral (1) can be found in [38]. For the case of finite horizon, the authors of [38] propose efficient ways to circumvent the problem of finding intersections between FEs and nonlocal neighborhoods by introducing the concept of "approximate balls" given by FE patches that roughly approximate $\mathcal{H}(\mathbf{x}, \delta)$; their results indicate that in the case of piecewise linear FE spaces, optimal numerical convergence can be preserved. Alternatively, in [49], the authors propose a technique that allows one to compute the inner integral over the whole element Ω_j^h by introducing a smoothing of the kernel function. The smoothed kernel is still compactly supported, but it continuously decays to zero, allowing for simple Gaussian quadrature rules over each FE.

In this work, under the assumption that the discretization parameter h (the size of the FE) and the nonlocal radius δ are proportional, we propose a change of perspective and introduce a technique where the inner integration is performed over the ball $\mathcal{H}(\mathbf{x}, \delta)$ rather than on a single element, i.e., the core computation in the stiffness matrix assembly now becomes

$$\int_{\Omega_i^h} \int_{\mathscr{H}(\mathbf{x},\delta)} [\psi_k(\mathbf{y}) - \psi_k(\mathbf{x})] \gamma(\mathbf{x},\mathbf{y}) [\psi_l(\mathbf{y}) - \psi_l(\mathbf{x})] \, d\mathbf{y} \, d\mathbf{x},\tag{2}$$

where we utilize special quadrature rules for the numerical computation of the inner integral. Specifically, we consider quadrature rules based on the generalized moving least squares (GMLS) method, successfully used for strong-form meshfree discretizations of nonlocal problems in [46,50,51]. The main idea behind this approach is to determine the quadrature weights associated with quadrature points (the meshfree discretization nodes in a meshfree setting) by solving an equality constrained optimization problem (see Section 3 for a thorough discussion). The introduction of a technique that fully circumvents the computation of element-ball intersections and that allows for the use of global quadrature rules over the support of the kernel function is the major contribution of this work. Additionally, the technique we propose requires minimal implementation effort, as the GMLS subroutine can be embedded into an existing FE code. As such, we envision this technique as a key component of agile FE engineering codes. In this work, we consider one- and two-dimensional implementations of piecewise linear continuous FE approximations. When boundary conditions are carefully treated and when the outer integral in (2) is accurately computed, this method is asymptotically compatible in the limit of h and δ vanishing and features first-order convergence in the L^2 norm for all dimensions and for both uniform and nonuniform grids. Furthermore, in the case of uniform grids, the proposed method is patch-test consistent (i.e., it is machine-precision accurate for linear solutions) and, according to numerical evidence, features an optimal, second-order convergence rate. Our numerical tests also indicate that, even for nonuniform grids, second-order convergence may be observed in the pre-asymptotic regime. Another contribution of the current work is a preliminary theoretical study, where, in a simplified, uniformly-discretized, one-dimensional setting, we show that the proposed method features optimal first-order numerical convergence in the H^1 norm. These results set the groundwork for more rigorous studies that we will pursue in future works.

Paper outline. Section 2 introduces the nonlocal Laplace operator and the corresponding volume-constrained nonlocal problem in its strong and weak form. Section 3 introduces the GMLS technique for the numerical evaluation of general integrals. In Section 4, we formulate the discrete variational problem for a FE discretization and we provide a detailed description of the quadrature rules and the resulting, fully-discrete problem. We also introduce a technique for the treatment of nonlocal boundary conditions that guarantees an improved convergence behavior. In Section 5, we introduce the concept of asymptotic compatibility and prove that, under certain assumptions, the proposed method features linear numerical convergence in the H^1 norm with respect to the mesh size (and, as a consequence, with respect to the interaction radius). Section 6 illustrates the accuracy of the proposed method with several one- and two-dimensional numerical tests on uniform and non-uniform grids using piecewise linear continuous FE discretizations. We first show the improved convergence behavior induced by the special treatment of the nonlocal boundary condition and then show that, in the L^2 norm, our scheme is second-order accurate for uniform discretizations and at least first-order accurate for non-uniform ones, with respect to h and δ and is, hence, asymptotically compatible. Moreover, we also show that convergence in the H^1 norm is consistent with the theoretical predictions discussed in Section 5. Lastly, we make some concluding remarks in Section 7.

2. Nonlocal Laplace operator and model problem

In this section we set the notation that will be used throughout the paper and introduce relevant definitions and results. In particular, we formulate the strong and weak forms of the nonlocal Poisson problem used to describe the technique proposed in this work.

Let $\gamma(\mathbf{x}, \mathbf{y}) : \mathbb{R}^d \times \mathbb{R}^d \to \mathbb{R}_0^+$ be a symmetric, i.e., $\gamma(\mathbf{x}, \mathbf{y}) = \gamma(\mathbf{y}, \mathbf{x})$, non-negative kernel with bounded support in the norm-induced ball of radius δ , i.e.,

$$\mathcal{H}(\mathbf{x}, \delta) := \operatorname{supp}(\gamma(\mathbf{x}, \cdot)) = \left\{ \mathbf{y} \in \mathbb{R}^d : |\mathbf{y} - \mathbf{x}|_{\ell^{\tilde{p}}} \le \delta \right\},\tag{3}$$

¹ Examples and analysis of nonsymmetric and sign-changing kernels can be found in [52,53] and [54], respectively.

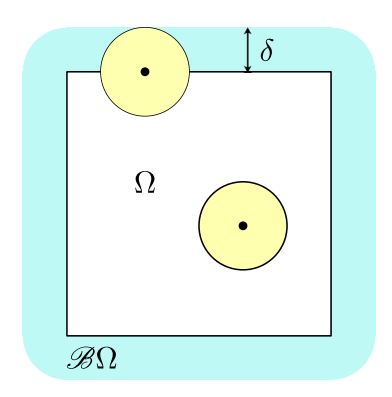


Fig. 1. A square domain Ω (in white) with its corresponding interaction domain of thickness δ (in light-blue). In yellow, two balls of radius δ , centered at two points in $\Omega \cup \mathcal{B}\Omega$, depicted by black dots, one of which is in Ω , while the other is located on the boundary $\partial \Omega$ between Ω and $\mathcal{B}\Omega$. (For interpretation of the references to color in this figure legend, the reader is referred to the web version of this article.)

where $\delta > 0$ is referred to as the *horizon* and $\tilde{p} \in [1, \infty]$. In this work, without loss of generality, we consider Euclidean balls, i.e., we take $\tilde{p} = 2$. Furthermore, we restrict ourselves to kernels of the form

$$\gamma(\mathbf{x}, \mathbf{y}) = \begin{cases}
\frac{\zeta_c}{\delta^{d+2}} & \text{for } |\mathbf{y} - \mathbf{x}|_{\ell\tilde{p}} \le \delta, \\
0 & \text{for } |\mathbf{y} - \mathbf{x}|_{\ell\tilde{p}} > \delta,
\end{cases}$$
(4)

and

$$\gamma(\mathbf{x}, \mathbf{y}) = \begin{cases}
\frac{\zeta_r}{\delta^{d+1} |\mathbf{y} - \mathbf{x}|_{\ell\tilde{p}}} & \text{for } |\mathbf{y} - \mathbf{x}|_{\ell\tilde{p}} \le \delta, \\
0 & \text{for } |\mathbf{y} - \mathbf{x}|_{\ell\tilde{p}} > \delta,
\end{cases} (5)$$

with ζ_c , $\zeta_r \in \mathbb{R}^+$.

Let $\Omega \subset \mathbb{R}^d$ be a bounded open domain. Its associated *interaction domain* is defined as the set of points outside of Ω that interact with points inside of it (see Fig. 1), i.e.,

$$\mathscr{B}\Omega := \left\{ \mathbf{y} \in \mathbb{R}^d \setminus \Omega : \exists \mathbf{x} \in \Omega \text{ such that } |\mathbf{y} - \mathbf{x}|_{\ell \tilde{p}} \le \delta \right\}. \tag{6}$$

Note that $\mathcal{B}\Omega \cap \partial\Omega = \partial\Omega$, where $\partial\Omega$ is the boundary of Ω [38].

We introduce the strong form of a nonlocal volume-constrained Poisson problem [37,50,55,56]: given $b: \Omega \to \mathbb{R}$ and $g: \mathcal{B}\Omega \to \mathbb{R}$, find $u: \Omega \cup \mathcal{B}\Omega \to \mathbb{R}$, such that

$$\begin{cases}
-\mathcal{L}_{\delta}u(\mathbf{x}) = b(\mathbf{x}), & \mathbf{x} \in \Omega, \\
u(\mathbf{x}) = g(\mathbf{x}), & \mathbf{x} \in \mathcal{B}\Omega,
\end{cases}$$
(7)

where $\mathcal{L}_{\delta}u(\mathbf{x})$ is the nonlocal Laplacian

$$\mathcal{L}_{\delta}u(\mathbf{x}) = 2 \int_{\Omega \cup \mathcal{B}\Omega} \gamma(\mathbf{x}, \mathbf{y})(u(\mathbf{y}) - u(\mathbf{x}))d\mathbf{y}, \tag{8}$$

and where the second equation is a *Dirichlet volume constraint*. In this work, we only consider Dirichlet constraints².

² Examples of the numerical treatment of Neumann constraints can be found in, e.g., [57,58]

2.1. Weak formulation

To derive the weak formulation associated with the problem in Eq. (7), we multiply the first equation in (7) by a test function $v(\mathbf{x}): \Omega \cup \mathcal{B}\Omega \to \mathbb{R}$ and then integrate over Ω , i.e.,

$$0 = \int_{\Omega} v(\mathbf{x}) \left[-\mathcal{L}_{\delta} u(\mathbf{x}) - b(\mathbf{x}) \right] d\mathbf{x}$$

$$= -2 \int_{\Omega} v(\mathbf{x}) \int_{\Omega \cup \mathscr{B}\Omega} \gamma(\mathbf{x}, \mathbf{y}) (u(\mathbf{y}) - u(\mathbf{x})) d\mathbf{y} d\mathbf{x} - \int_{\Omega} v(\mathbf{x}) b(\mathbf{x}) d\mathbf{x}.$$
(9)

Now we recast $-2\int_{\Omega} v(\mathbf{x}) \int_{\Omega \cup \mathcal{B}\Omega} \gamma(\mathbf{x}, \mathbf{y}) (u(\mathbf{y}) - u(\mathbf{x})) d\mathbf{y} d\mathbf{x}$ as

$$-2\int_{\Omega} v(\mathbf{x}) \int_{\Omega \cup \mathcal{B}\Omega} \gamma(\mathbf{x}, \mathbf{y})(u(\mathbf{y}) - u(\mathbf{x})) d\mathbf{y} d\mathbf{x}$$

$$= -2\int_{\Omega} v(\mathbf{x}) \int_{\Omega \cup \mathcal{B}\Omega} \frac{1}{2} \left[\gamma(\mathbf{x}, \mathbf{y})(u(\mathbf{y}) - u(\mathbf{x})) - \gamma(\mathbf{x}, \mathbf{y})(u(\mathbf{x}) - u(\mathbf{y})) \right] d\mathbf{y} d\mathbf{x}$$

$$= -\int_{\Omega} v(\mathbf{x}) \int_{\Omega \cup \mathcal{B}\Omega} \left[\gamma(\mathbf{x}, \mathbf{y})(u(\mathbf{y}) - u(\mathbf{x})) - \gamma(\mathbf{y}, \mathbf{x})(u(\mathbf{x}) - u(\mathbf{y})) \right] d\mathbf{y} d\mathbf{x},$$
(10)

where we employed the symmetry of γ . As is standard in the presence of Dirichlet conditions, we require $v(\mathbf{x})$ to be zero on $\mathcal{B}\Omega$. We then apply *Green's first identity of nonlocal vector calculus* [56] to the term in Eq. (10), which gives us, with $v(\mathbf{x}) = 0$ for $\mathbf{x} \in \mathcal{B}\Omega$,

$$-\int_{\Omega} v(\mathbf{x}) \int_{\Omega \cup \mathcal{B}\Omega} \left[\gamma(\mathbf{x}, \mathbf{y})(u(\mathbf{y}) - u(\mathbf{x})) - \gamma(\mathbf{y}, \mathbf{x})(u(\mathbf{x}) - u(\mathbf{y})) \right] d\mathbf{y} d\mathbf{x}$$

$$= \int_{\Omega \cup \mathcal{B}\Omega} \int_{\Omega \cup \mathcal{B}\Omega} \left[v(\mathbf{y}) - v(\mathbf{x}) \right] \gamma(\mathbf{x}, \mathbf{y}) \left[u(\mathbf{y}) - u(\mathbf{x}) \right] d\mathbf{y} d\mathbf{x}.$$
(11)

Therefore, by combining Eqs. (10) and (11) we get

$$-2\int_{\Omega} v(\mathbf{x}) \int_{\Omega \cup \mathcal{B}\Omega} \gamma(\mathbf{x}, \mathbf{y})(u(\mathbf{y}) - u(\mathbf{x})) d\mathbf{y} d\mathbf{x}$$

$$= \int_{\Omega \cup \mathcal{B}\Omega} \int_{\Omega \cup \mathcal{B}\Omega} \left[v(\mathbf{y}) - v(\mathbf{x}) \right] \gamma(\mathbf{x}, \mathbf{y}) \left[u(\mathbf{y}) - u(\mathbf{x}) \right] d\mathbf{y} d\mathbf{x}.$$
(12)

By substituting the latter in Eq. (9), we obtain

$$\int_{\Omega \cup \mathcal{B}\Omega} \int_{\Omega \cup \mathcal{B}\Omega} \left[v(\mathbf{y}) - v(\mathbf{x}) \right] \gamma(\mathbf{x}, \mathbf{y}) \left[u(\mathbf{y}) - u(\mathbf{x}) \right] d\mathbf{y} d\mathbf{x} = \int_{\Omega} v(\mathbf{x}) b(\mathbf{x}) d\mathbf{x}. \tag{13}$$

By defining the bilinear form $D(\cdot, \cdot)$ and the linear functional $G(\cdot)$ as

$$D(u, v) := \int_{\Omega \cup \mathscr{B}\Omega} \int_{\Omega \cup \mathscr{B}\Omega} \left[v(\mathbf{y}) - v(\mathbf{x}) \right] \gamma(\mathbf{x}, \mathbf{y}) \left[u(\mathbf{y}) - u(\mathbf{x}) \right] d\mathbf{y} d\mathbf{x}, \tag{14}$$

and

$$G(v) := \int_{\mathcal{O}} v(\mathbf{x})b(\mathbf{x})d\mathbf{x},\tag{15}$$

we can rewrite Eq. (13) as

$$D(u,v) = G(v). (16)$$

In double integral operators of the form $\int (\int (...) d\mathbf{y}) d\mathbf{x}$, we refer to $\int (...) d\mathbf{y}$ as the *inner integral*, and to $\int (...) d\mathbf{x}$ as the *outer integral*.

We define the following function spaces for functions $w(\mathbf{x})$ defined for $\mathbf{x} \in \Omega \cup \mathcal{B}\Omega$:

$$\mathcal{V}(\Omega \cup \mathcal{B}\Omega) := \left\{ w \in L^2(\Omega \cup \mathcal{B}\Omega) : ||w|| < \infty \right\},\tag{17}$$

where we define the norm

$$\|w\|^{2} = \int_{\Omega \cup \mathcal{B}\Omega} \int_{\Omega \cup \mathcal{B}\Omega} |w(\mathbf{y}) - w(\mathbf{x})|^{2} \gamma(\mathbf{x}, \mathbf{y}) d\mathbf{y} d\mathbf{x} + \|w\|_{L^{2}(\Omega \cup \mathcal{B}\Omega)}^{2}$$

$$= D(w, w) + \|w\|_{L^{2}(\Omega \cup \mathcal{B}\Omega)}^{2}.$$
(18)

We also introduce the constrained energy space

$$\mathcal{V}_0(\Omega \cup \mathcal{B}\Omega) := \{ w \in \mathcal{V}(\Omega \cup \mathcal{B}\Omega) : w|_{\mathcal{B}\Omega} = 0 \}, \tag{19}$$

for which

$$||w||_0^2 = D(w, w),$$
 (20)

defines a norm. Finally, we define the nonlocal trace space as $\mathcal{V}_t(\Omega \cup \mathcal{B}\Omega) = \{w|_{\mathcal{B}\Omega} : w \in \mathcal{V}(\Omega \cup \mathcal{B}\Omega)\}$. Let $\mathcal{V}' : \mathcal{V}_0 \to \mathbb{R}$ denote the dual space of bounded linear functionals on \mathcal{V}_0 via L^2 duality pairing, i.e., the space of functionals $\varphi : \mathcal{V}_0 \times \mathcal{W} \to \mathbb{R}$ of the type

$$\varphi(\cdot, \cdot) = \int_{\Omega} (\cdot)(\cdot) d\mathbf{x},\tag{21}$$

where $W: \Omega \to \mathbb{R}$. Thus, $\forall w \in \mathcal{W}(\Omega)$, we can write $\varphi(\cdot, w): \mathcal{V}_0 \to \mathbb{R} \in \mathcal{V}'$ as

$$\varphi(\cdot, w) = \int_{\Omega} (\cdot) w(\mathbf{x}) d\mathbf{x}. \tag{22}$$

By comparing Eqs. (15) and (22) we see that $G(\cdot) = \varphi(\cdot, w)$, $\forall w \in \mathcal{W}(\Omega)$. Then, the weak form of (7) is defined as follows: given $g(\mathbf{x}) \in \mathcal{V}_t(\Omega \cup \mathcal{B}\Omega)$, and $b(\mathbf{x}) \in \mathcal{W}(\Omega)$, find $u(\mathbf{x}) \in \mathcal{V}(\Omega \cup \mathcal{B}\Omega)$ such that $\forall v(\mathbf{x}) \in \mathcal{V}_0(\Omega \cup \mathcal{B}\Omega)$

$$D(u, v) = G(v), \tag{23}$$

subject to $u(\mathbf{x}) = g(\mathbf{x})$ for $\mathbf{x} \in \mathcal{B}\Omega$. Discussions on the well-posedness of (23) can be found in [37,55].

3. Quadrature weights using generalized moving least squares

In this section we review the quadrature approach based on the generalized moving least squares (GMLS) [59–61] method, proposed in [46]. For given positions of quadrature points, this method determines their associated quadrature weights by solving an equality constrained optimization problem. In [46], the GMLS-based quadrature was employed within the framework of collocation-based meshfree discretizations of strong-form nonlocal problems.

Consider a collection of points $\mathbf{X}_p = \{\mathbf{x}_j\}_{j=1,\dots,N_p} \subset \mathcal{H}(\mathbf{x},\delta)$, with $N_p \in \mathbb{N}$, and a quadrature rule for functions $f(\mathbf{x},\mathbf{y}) \in \mathbf{V}$, given by

$$\int_{\mathscr{H}(\mathbf{x},\delta)} f(\mathbf{x},\mathbf{y}) d\mathbf{y} \approx \sum_{\substack{j=1\\j:\mathbf{x}_{j}\neq\mathbf{x}}}^{N_{p}} f_{j}\omega_{j},\tag{24}$$

where **V** denotes a Banach space, $f_j = f(\mathbf{x}, \mathbf{x}_j)$, and $\{\omega_j\}_{j=1,\dots,N_p} \in \mathbb{R}^{N_p}$ is a collection of quadrature weights to be determined. Notice that in Eq. (24) we are excluding $\mathbf{x}_j = \mathbf{x}$ to account for the possibility of $f(\mathbf{x}, \mathbf{y})$ having a singularity when $\mathbf{x} = \mathbf{x}_j = \mathbf{y}$. If the function does not exhibit such singularity, then $\mathbf{x}_j = \mathbf{x}$ could also be included in the summation. In order to find the quadrature weights we define the following equality constrained optimization problem: find

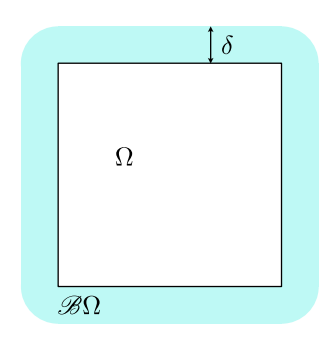
$$\underset{\{\omega_j\}\in\mathbb{R}^{N_p}}{\operatorname{argmin}} \sum_{\substack{j=1\\j:\mathbf{x}_j\neq\mathbf{x}}}^{N_p} \omega_j^2 \tag{25}$$

subject to
$$\sum_{\substack{j=1\\j;\mathbf{x}_i\neq\mathbf{x}}}^{N_p} f_j \omega_j = \int_{\mathscr{H}(\mathbf{x},\delta)} f(\mathbf{x},\mathbf{y}) d\mathbf{y} \ \forall f \in \mathbf{V}_h \subset \mathbf{V},$$

where V_h is a finite dimensional subspace of V, consisting of functions to be integrated exactly. The problem in (25) leads to the following saddle-point problem:

$$\begin{bmatrix} \mathbf{I} & \mathbf{B}^T \\ \mathbf{B} & \mathbf{0} \end{bmatrix} \begin{bmatrix} \boldsymbol{\omega} \\ \boldsymbol{\lambda} \end{bmatrix} = \begin{bmatrix} \mathbf{0} \\ \mathbf{g} \end{bmatrix}, \tag{26}$$

where $\mathbf{I} \in \mathbb{R}^{N_p \times N_p}$ is the identity matrix; $\boldsymbol{\omega} = \{\omega_j\}_{j=1,\dots,N_p} \in \mathbb{R}^{N_p}$ is the vector containing the set of quadrature weights; and $\boldsymbol{\lambda} \in \mathbb{R}^{\dim(\mathbf{V}_h)}$ is the vector of Lagrange multipliers enforcing the constraint. $\mathbf{B} \in \mathbb{R}^{N_p \times \dim(\mathbf{V}_h)}$ is defined



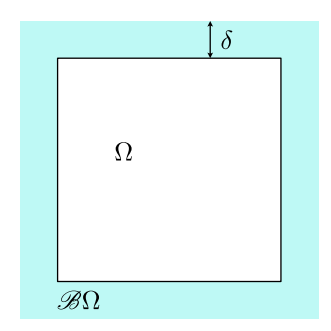


Fig. 2. Left: a square domain Ω (in white) with its corresponding interaction domain $\mathcal{B}\Omega$ (in light-blue). Right: the same square domain and a polygonal approximate interaction domain, still referred to as $\mathcal{B}\Omega$. (For interpretation of the references to color in this figure legend, the reader is referred to the web version of this article.)

by $B_{aj} = f^{\alpha}(\mathbf{x}, \mathbf{x}_j)$, $\forall f^{\alpha} \in \mathbf{V}_h$, where $\{f^{\alpha}\}_{\alpha=1,\dots,\dim(\mathbf{V}_h)}$ is a basis of \mathbf{V}_h . The vector $\mathbf{g} \in \mathbb{R}^{\dim(\mathbf{V}_h)}$ contains the exact integrals of each function in $\{f^{\alpha}\}_{\alpha=1,\dots,\dim(\mathbf{V}_h)}$, i.e., $g_{\alpha} = \int_{\mathscr{H}(\mathbf{x},\delta)} f^{\alpha}(\mathbf{x},\mathbf{y}) d\mathbf{y}$. Based on Eq. (26), the quadrature weights can be obtained as

$$\boldsymbol{\omega} = \mathbf{B}^{\mathsf{T}} \mathbf{S}^{\mathsf{+}} \mathbf{g},\tag{27}$$

where $S = BB^T$ and S^+ is the Moore–Penrose inverse of S. It has to be noted that the set of integration weights for a given constraint might not be unique [39,50] and that redundant (linearly dependent) conditions might be present in the constraints. This results in the singularity of the matrix S. In this work, as in [46], a pseudoinverse, such as S^+ , is used to compute S^{-1} , whenever S is singular. It should also be noted that, as discussed in [39,50], this set of integration weights can be constructed equivalently by using the reproducing kernel particle method (RKPM) [62], due to the equivalence of RKPM and GMLS.

4. Discrete variational form

In this section we introduce the discrete form of the variational problem in Eq. (23); specifically, for piecewise linear, finite element discretizations, we describe the computational domain, the discrete representation of the unknown field $u(\mathbf{x})$ and the trial function $v(\mathbf{x})$, and the quadrature rules utilized for the numerical evaluation of the integrals.

4.1. Finite element discretization of the weak formulation

Let $\mathcal{M}_{\Omega}^h := \{\Omega_e^h\}_{e=1,\dots,n_{el,\Omega}}, \ n_{el,\Omega} \in \mathbb{N}$, be a collection of non-overlapping elements, which are open, simply connected subsets of \mathbb{R}^d , and let $\partial \Omega_e^h$ be their corresponding boundary. Therefore, $\Omega_i^h \cap \Omega_j^h = \varnothing$ and $\overline{\Omega_i^h} \cap \overline{\Omega_j^h} = \partial \Omega_i^h \cap \partial \Omega_j^h$ with $i \neq j, i, j = 1, \dots, n_{el}$, where the bar denotes the closure of the set. We assume that the domain Ω , introduced in Section 2, is a polyhedral so that it can be exactly covered by the mesh \mathcal{M}_{Ω}^h , i.e., $\overline{\Omega} = \bigcup_{e=1}^{n_{el},\Omega} \overline{\Omega_e^h}$. Note that when Ω is not polyhedral, one can introduce a polyhedral approximation $\Omega^h \approx \Omega$ for which a covering exists. When the nonlocal interaction region is a Euclidean ball, the interaction domain $\mathcal{B}\Omega$ is generally not a polyhedral domain since vertices of Ω create rounded corners in $\mathcal{B}\Omega$ (see, for example, Fig. 1). Therefore, following [38], we approximate $\mathcal{B}\Omega$ by a polyhedral domain by replacing rounded corners by vertices (see Fig. 2 for illustration). From now on, we will refer to this approximate polyhedral domain also as $\mathcal{B}\Omega$. Note that there is no need to extend the boundary data $g(\mathbf{x})$ to added regions between the original curved corners and the new corners of the polyhedral approximation since these portions of the domain are never accessed during the numerical solution process.

Since we consider a polyhedral $\mathcal{B}\Omega$, we can construct another exact mesh $\mathcal{M}^h_{\mathcal{B}\Omega} := \{\Omega_e^h\}_{e=n_{el,\Omega}+1,\dots,n_{el}}$ containing $n_{el}-n_{el,\Omega}$ elements, i.e., $\overline{\mathcal{B}\Omega^h} := \bigcup_{e=n_{el,\Omega}+1}^{n_{el}-n_{el,\Omega}} \overline{\Omega_e^h} = \overline{\mathcal{B}\Omega}$, with $n_{el} \in \mathbb{N}$. Meshing Ω and $\mathcal{B}\Omega$ separately guarantees that elements do not straddle the shared boundary between Ω and $\mathcal{B}\Omega$, i.e., $\partial \Omega = \overline{\Omega} \cap \mathcal{B}\Omega$.

Moreover, we require that the vertices of the elements of $\mathcal{M}_{\mathcal{B}\Omega}^h$ and \mathcal{M}_{Ω}^h coincide along the boundary $\partial\Omega$, so that $\mathcal{M}^h = \mathcal{M}_{\Omega}^h \cup \mathcal{M}_{\mathcal{B}\Omega}^h = \{\Omega_e^h\}_{e=1}^{n_{el}}$ is a regular mesh for $\Omega \cup \mathcal{B}\Omega$.

We consider continuous finite element spaces with Lagrange-type compactly supported linear polynomial bases defined with respect to the nodes of \mathcal{M}^h . With $J \in \mathbb{N}$ and $J_{\Omega} \in \mathbb{N}$, let $\{\tilde{\mathbf{x}}_j\}_{j=1}^J$ be the set of all the nodes in \mathcal{M}^h , with $\{\tilde{\mathbf{x}}_j\}_{j=1}^{J_{\Omega}}$ and $\{\tilde{\mathbf{x}}_j\}_{j=J_{\Omega}+1}^J$ being the subset of nodes located in the open domain Ω and in the closed domain $\mathcal{B}\Omega$, respectively. Notice that in this way, the nodes located on $\partial \Omega = \overline{\Omega} \cap \mathcal{B}\Omega$ are assigned to $\mathcal{B}\Omega$. Then, for $j=1,\ldots,J$, let $\psi_j(\mathbf{x})$ denote a piecewise linear polynomial function such that $\psi_j(\tilde{\mathbf{x}}_k)=\delta_{jk}$ for $k=1,\ldots,J$, where δ_{ik} is the Kronecker delta function. Then, we define the finite element spaces as

$$\mathcal{V}^h = \operatorname{span}\{\psi_j\}_{j=1}^J \subset \mathcal{V}(\Omega \cup \mathcal{B}\Omega),\tag{28}$$

and

$$\mathcal{V}_0^h = \operatorname{span}\{\psi_j\}_{j=1}^{J_{\Omega}} \subset \mathcal{V}_0(\Omega \cup \mathcal{B}\Omega),\tag{29}$$

of dimensions J and J_{Ω} , respectively. Note that all functions belonging to \mathcal{V}^h and \mathcal{V}^h_0 are continuous by construction. The finite element approximation $u^h(\mathbf{x}) \in \mathcal{V}^h$ of the solution $u(\mathbf{x})$ of the nonlocal problem is defined as

$$u^{h}(\mathbf{x}) = \sum_{j=1}^{J} \psi_{j}(\mathbf{x})u_{j} = \sum_{j=1}^{J_{\Omega}} \psi_{j}(\mathbf{x})u_{j} + \sum_{j=J_{\Omega}+1}^{J} \psi_{j}(\mathbf{x})g(\tilde{\mathbf{x}}_{j}) = w^{h} + g^{h},$$
(30)

for a set of coefficients $\{u_j\}_{j=1}^J$. Here, the volume constraint in (7) has been applied to a subset associated with the nodes in $\mathcal{B}\Omega$

$$u_j = g(\tilde{\mathbf{x}}_j) \quad \text{for } j = J_{\Omega} + 1, \dots, J,$$
 (31)

so that

$$w^h := \sum_{j=1}^{J_{\Omega}} \psi_j(\mathbf{x}) u_j \quad \text{and} \quad g^h := \sum_{j=J_{\Omega}+1}^J \psi_j(\mathbf{x}) g(\tilde{\mathbf{x}}_j). \tag{32}$$

The finite element approximation u^h associated with the nonlocal problem in (23) is then found by solving the following discrete weak formulation: given $g(\mathbf{x}) \in \mathcal{V}_t(\Omega \cup \mathcal{B}\Omega)$, and $b(\mathbf{x}) \in \mathcal{W}(\Omega)$ (see Section 2.1), find $u^h \in \mathcal{V}^h$ such that $\forall v^h \in \mathcal{V}_0^h$

$$D(u^h, v^h) = G(v^h). (33)$$

By substituting Eq. (30) in Eq. (33) and by choosing $v^h(\mathbf{x})$ from the set of basis functions $\{\psi_i\}_{i=1}^{J_\Omega}$ we get

$$D(w^h, v^h) = G(v^h) - D(g^h, v^h), (34)$$

which results in the linear system

$$\sum_{j=1}^{J_{\Omega}} D(\psi_j, \psi_i) u_j = G(\psi_i) - D(g^h, \psi_i), \tag{35}$$

for $i = 1, ..., J_{\Omega}$. Eq. (35) can be expressed in matrix form as

$$\mathbf{A}\mathbf{u} = \mathbf{f},\tag{36}$$

where **A** is a $J_{\Omega} \times J_{\Omega}$ matrix with components

$$A_{ij} = D(\psi_j, \psi_i)$$

$$= \int_{\Omega \cup \mathcal{B}\Omega} \int_{\Omega \cup \mathcal{B}\Omega} [\psi_i(\mathbf{y}) - \psi_i(\mathbf{x})] \gamma(\mathbf{x}, \mathbf{y}) [\psi_j(\mathbf{y}) - \psi_j(\mathbf{x})] d\mathbf{y} d\mathbf{x},$$
(37)

f is a $J_{\Omega} \times 1$ vector with components

$$f_{i} = G(\psi_{i}) - D(g^{h}, \psi_{i}) = \int_{\Omega} \psi_{i}(\mathbf{x})b(\mathbf{x})d\mathbf{x}$$

$$- \int_{\Omega \cup \mathcal{B}\Omega} \int_{\Omega \cup \mathcal{B}\Omega} \left[\psi_{i}(\mathbf{y}) - \psi_{i}(\mathbf{x}) \right] \gamma(\mathbf{x}, \mathbf{y}) \left[g^{h}(\mathbf{y}) - g^{h}(\mathbf{x}) \right] d\mathbf{y}d\mathbf{x},$$
(38)

and **u** is a vector of size $J_{\Omega} \times 1$ containing the set of unknown coefficients $\{u_i\}_{i=1}^{J_{\Omega}}$ to be determined.

4.2. Discrete quadrature

We introduce the numerical quadrature used to solve Eq. (34). As described in Section 4.1 we discretize $\Omega \cup \mathcal{B}\Omega$ using the mesh \mathcal{M}^h , and Ω with $M_{\Omega}^h \subset \mathcal{M}^h$. Therefore, we can express the left-hand side (LHS) and the right-hand side (RHS) of Eq. (34) as

$$D(w^{h}, v^{h})$$

$$= \int_{\Omega \cup \mathcal{B}\Omega} \int_{\Omega \cup \mathcal{B}\Omega} \left[v^{h}(\mathbf{y}) - v^{h}(\mathbf{x}) \right] \gamma(\mathbf{x}, \mathbf{y}) \left[w^{h}(\mathbf{y}) - w^{h}(\mathbf{x}) \right] d\mathbf{y} d\mathbf{x}$$

$$= \sum_{\Omega_{e}^{h} \in \mathcal{M}^{h}} \int_{\Omega_{e}^{h}} \int_{\Omega \cup \mathcal{B}\Omega} \left[v^{h}(\mathbf{y}) - v^{h}(\mathbf{x}) \right] \gamma(\mathbf{x}, \mathbf{y}) \left[w^{h}(\mathbf{y}) - w^{h}(\mathbf{x}) \right] d\mathbf{y} d\mathbf{x}$$

$$= \sum_{\Omega_{e}^{h} \in \mathcal{M}^{h}} \int_{\Omega_{e}^{h}} \int_{\Omega \cup \mathcal{B}\Omega \cap \mathcal{H}(\mathbf{x}, \delta)} \left[v^{h}(\mathbf{y}) - v^{h}(\mathbf{x}) \right] \gamma(\mathbf{x}, \mathbf{y}) \left[w^{h}(\mathbf{y}) - w^{h}(\mathbf{x}) \right] d\mathbf{y} d\mathbf{x},$$
(39)

and

$$G(v^{h}) - D(g^{h}, v^{h})$$

$$= \int_{\Omega} v^{h}(\mathbf{x})b(\mathbf{x})d\mathbf{x}$$

$$- \int_{\Omega \cup \mathscr{B}\Omega} \int_{\Omega \cup \mathscr{B}\Omega} \left[v^{h}(\mathbf{y}) - v^{h}(\mathbf{x}) \right] \gamma(\mathbf{x}, \mathbf{y}) \left[g^{h}(\mathbf{y}) - g^{h}(\mathbf{x}) \right] d\mathbf{y} d\mathbf{x}$$

$$= \sum_{\Omega_{e}^{h} \in \mathcal{M}_{\Omega}^{h}} \int_{\Omega_{e}^{h}} v^{h}(\mathbf{x})b(\mathbf{x})d\mathbf{x}$$

$$- \sum_{\Omega_{e}^{h} \in \mathcal{M}^{h}} \int_{\Omega_{e}^{h}} \int_{(\Omega \cup \mathscr{B}\Omega) \cap \mathscr{H}(\mathbf{x}, \delta)} \left[v^{h}(\mathbf{y}) - v^{h}(\mathbf{x}) \right] \gamma(\mathbf{x}, \mathbf{y}) \left[g^{h}(\mathbf{y}) - g^{h}(\mathbf{x}) \right] d\mathbf{y} d\mathbf{x},$$

$$(40)$$

where we have restricted the inner integral to $(\Omega \cup \mathcal{B}\Omega) \cap \mathcal{H}(\mathbf{x}, \delta)$ (see Eq. (3)).

We now describe how to discretize the integrals over the mesh elements Ω_e^h and over $(\Omega \cup \mathcal{B}\Omega) \cap \mathcal{H}(\mathbf{x}, \delta)$. For the outer integral (over the elements) we consider a high-order Gauss quadrature; for further discussion on outer quadrature schemes we refer the reader to [38]. For $N_q \in \mathbb{N}$, we denote the set of element Gauss quadrature points and weights to be used for the element integrals present in $D(w^h, v^h)$ as $\{\mathbf{x}_q^e\}_{q=1}^{N_q} \in \Omega_e^h$ and $\{\omega_q^e\}_{q=1}^{N_q}$, respectively. We also define, for $N_b \in \mathbb{N}$, the set of element Gauss quadrature points and weights to be employed for the integration over the elements in $G(v^h)$ as $\{\mathbf{x}_b^e\}_{b=1}^{N_b} \in \Omega_e^h$ and $\{\omega_b^e\}_{b=1}^{N_b}$, respectively. Therefore, from Eqs. (39) and (40), we get

$$D(w^{h}, v^{h}) = \sum_{\Omega_{e}^{h} \in \mathcal{M}^{h}} \int_{\Omega_{e}^{h}} \int_{(\Omega \cup \mathcal{B}\Omega) \cap \mathcal{H}(\mathbf{x}, \delta)} \left[v^{h}(\mathbf{y}) - v^{h}(\mathbf{x}) \right] \gamma(\mathbf{x}, \mathbf{y}) \left[w^{h}(\mathbf{y}) - w^{h}(\mathbf{x}) \right] d\mathbf{y} d\mathbf{x}$$

$$\approx \sum_{\Omega^{h} \in \mathcal{M}^{h}} \sum_{q=1}^{N_{q}} \int_{(\Omega \cup \mathcal{B}\Omega) \cap \mathcal{H}(\mathbf{x}_{q}^{e}, \delta)} \left[v^{h}(\mathbf{y}) - v^{h}(\mathbf{x}_{q}^{e}) \right] \gamma(\mathbf{x}_{q}^{e}, \mathbf{y}) \left[w^{h}(\mathbf{y}) - w^{h}(\mathbf{x}_{q}^{e}) \right] d\mathbf{y} \omega_{q}^{e},$$

$$(41)$$

Fig. 3. One-dimensional Euclidean ball quadrature points. The filled red dot represents x_q^e while the blue crosses are the associated quadrature points x_{ap}^e .

and

$$G(v^{h}) - D(g^{h}, v^{h})$$

$$= \sum_{\Omega_{e}^{h} \in \mathcal{M}_{\Omega}^{h}} \int_{\Omega_{e}^{h}} v^{h}(\mathbf{x})b(\mathbf{x})d\mathbf{x} - \sum_{\Omega_{e}^{h} \in \mathcal{M}^{h}} \int_{\Omega_{e}^{h}} \int_{(\Omega \cup \mathcal{B}\Omega) \cap \mathcal{H}(\mathbf{x}, \delta)} \left[v^{h}(\mathbf{y}) - v^{h}(\mathbf{x}) \right] \gamma(\mathbf{x}, \mathbf{y}) \left[g^{h}(\mathbf{y}) - g^{h}(\mathbf{x}) \right] d\mathbf{y} d\mathbf{x}$$

$$\approx \sum_{\Omega_{e}^{h} \in \mathcal{M}_{\Omega}^{h}} \sum_{b=1}^{N_{b}} v^{h}(\mathbf{x}_{b}^{e})b(\mathbf{x}_{b}^{e})\omega_{b}^{e} - \sum_{\Omega_{e}^{h} \in \mathcal{M}^{h}} \sum_{q=1}^{N_{q}} \int_{(\Omega \cup \mathcal{B}\Omega) \cap \mathcal{H}(\mathbf{x}_{q}^{e}, \delta)} \left[v^{h}(\mathbf{y}) - v^{h}(\mathbf{x}_{q}^{e}) \right] \gamma(\mathbf{x}_{q}^{e}, \mathbf{y}) \left[g^{h}(\mathbf{y}) - g^{h}(\mathbf{x}_{q}^{e}) \right] d\mathbf{y} \omega_{q}^{e}.$$

$$(42)$$

To discretize the remaining inner integrals over $(\Omega \cup \mathcal{B}\Omega) \cap \mathcal{H}(\mathbf{x}_q^e, \delta)$ in Eqs. (41) and (42) we use the GMLS quadrature introduced in Section 3. We start with the case in which $(\Omega \cup \mathcal{B}\Omega) \cap \mathcal{H}(\mathbf{x}_q^e, \delta) = \mathcal{H}(\mathbf{x}_q^e, \delta)$, i.e., the integration domain is the full ball of radius δ around \mathbf{x}_q^e . Note that this is the case for all $\mathbf{x}_q^e \in (\Omega \cup \partial \Omega)$. We then consider the following set of points placed in a regular uniform grid, symmetric around \mathbf{x}_q^e :

$$\begin{aligned}
\left\{\mathbf{x}_{qp}^{e}\right\}_{p=1}^{\overline{N}_{qp}} &:= \left\{\mathbf{x}_{qp}^{e} \in \mathbb{R}^{d}; k_{1}, k_{2}, \dots, k_{d} \in \mathbb{Z} \setminus \{0\} : \mathbf{x}_{qp}^{e} = \left(x_{qp1}^{e}, x_{qp2}^{e}, \dots, x_{qpd}^{e}\right) \\
&= \left(x_{q1}^{e} + (2k_{1} - \operatorname{sgn}(k_{1}))\frac{\overline{h}}{2}, x_{q2}^{e} + (2k_{2} - \operatorname{sgn}(k_{2}))\frac{\overline{h}}{2}, \dots, x_{qd}^{e} + (2k_{d} - \operatorname{sgn}(k_{d}))\frac{\overline{h}}{2}\right), \\
&- \overline{N}_{qp,\delta} \leq k_{1}, k_{2}, \dots, k_{d} \leq \overline{N}_{qp,\delta} \right\},
\end{aligned} \tag{43}$$

where $\overline{N}_{qp,\delta} \in \mathbb{N}$,

$$\overline{h} = \frac{\delta}{\overline{N}_{qp,\delta}} \tag{44}$$

is the spacing between grid points, and

$$\overline{N}_{qp} = \left(2\overline{N}_{qp,\delta}\right)^d,\tag{45}$$

is the overall number of points. In this work, we take $\overline{N}_{qp,\delta}$ to be a constant independent of q, i.e., $\overline{N}_{q_ip,\delta} = \overline{N}_{q_jp,\delta}$ $\forall q_i, q_j$ such that $\mathbf{x}_{q_i}^e, \mathbf{x}_{q_j}^e \in \Omega \cup \mathcal{B}\Omega$. The subset of N_{qp} points of $\{\mathbf{x}_{qp}^e\}_{p=1}^{\overline{N}_{qp}}$ contained in $\mathcal{H}(\mathbf{x}_q^e, \delta) \cap (\Omega \cup \mathcal{B}\Omega)$ is given by

$$\begin{aligned}
\left\{\mathbf{x}_{qp}^{e}\right\}_{p=1}^{N_{qp}} &:= \left\{\mathbf{x}_{qp}^{e}\right\}_{p=1}^{\overline{N}_{qp}} \cap \mathcal{H}(\mathbf{x}_{q}^{e}, \delta) \cap (\Omega \cup \mathcal{B}\Omega) \\
&= \left\{\mathbf{x}_{qp}^{e} \in \left\{\mathbf{x}_{qp}^{e}\right\}_{p=1}^{\overline{N}_{qp}} \cap (\Omega \cup \mathcal{B}\Omega) : |\mathbf{x}_{qp}^{e} - \mathbf{x}_{q}^{e}|_{\ell^{\bar{p}}} \leq \delta \right\}.
\end{aligned} \tag{46}$$

This is the set of quadrature points used to discretize the integrals over $(\Omega \cup \mathcal{B}\Omega) \cap \mathcal{H}(\mathbf{x}_q^e, \delta)$ in Eqs. (41) and (42). When $(\Omega \cup \mathcal{B}\Omega) \cap \mathcal{H}(\mathbf{x}_q^e, \delta) = \mathcal{H}(\mathbf{x}_q^e, \delta)$, this set reduces to

$$\left\{ \mathbf{x}_{qp}^{e} \right\}_{p=1}^{N_{qp}} = \left\{ \mathbf{x}_{qp}^{e} \in \left\{ \mathbf{x}_{qp}^{e} \right\}_{p=1}^{\overline{N}_{qp}} : |\mathbf{x}_{qp}^{e} - \mathbf{x}_{q}^{e}|_{\ell^{\tilde{p}}} \le \delta \right\}. \tag{47}$$

Figs. 3 and 4 show the distribution of quadrature points for one-dimensional and two-dimensional Euclidean balls. To determine the set of quadrature weights $\{\omega_{qp}^e\}_{p=1}^{N_{qp}}$ associated with $\{\mathbf{x}_{qp}^e\}_{p=1}^{N_{qp}}$, we employ the approach presented in Section 3, with $\mathbf{x} = \mathbf{x}_q^e$. As our finite dimensional space \mathbf{V}_h , i.e., as the space of functions for which

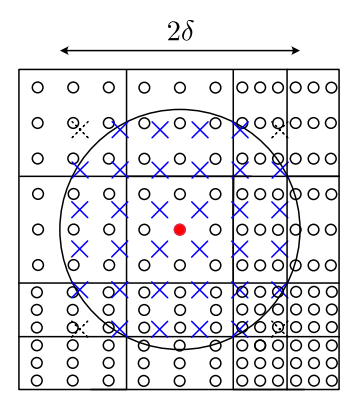


Fig. 4. Two-dimensional Euclidean ball quadrature points. The filled red dot represents \mathbf{x}_q^e while the blue crosses are the associated quadrature points \mathbf{x}_{qp}^e .

we impose exactness of integration, we select

$$\mathbf{V}_{h} = \{ f(\mathbf{x}, \mathbf{y}) : \Omega \cup \mathcal{B}\Omega \times \Omega \cup \mathcal{B}\Omega \to \mathbb{R}, f(\mathbf{x}, \mathbf{y}) = \gamma(\mathbf{x}, \mathbf{y}) (\mathbf{y} - \mathbf{x})^{\boldsymbol{\beta}} \text{ with } |\boldsymbol{\beta}| = 2 \},$$

$$(48)$$

where we are using multi-index notation. Here, $\boldsymbol{\beta}$ is a collection of d non-negative integers, $\boldsymbol{\beta}=(\beta_1,\ldots,\beta_d)$ with length $|\boldsymbol{\beta}|=\sum_{i=1}^d\beta_i$. For a given $\boldsymbol{\beta}$, $(\mathbf{y}-\mathbf{x})^{\boldsymbol{\beta}}=(y_1-x_1)^{\beta_1}\ldots(y_d-x_d)^{\beta_d}$. Eq. (48) can be related to assuming the trial and test functions $v(\mathbf{x})$ and $u(\mathbf{x})$ to be linear functions in Eqs. (41) and (42), consistently with our choice to approximate them with linear finite element approximations (see Section 4.1). In fact, in a one-dimensional case, Eq. (48) corresponds to imposing exact integration of $\int_{(\Omega\cup\mathcal{B}\Omega)\cap\mathcal{H}(\mathbf{x},\delta)}(y-x)\gamma(x,y)(y-x)dy$, while in a two-dimensional case, to imposing exact integration of $\int_{(\Omega\cup\mathcal{B}\Omega)\cap\mathcal{H}(\mathbf{x},\delta)}(y_1-x_1)\gamma(\mathbf{x},\mathbf{y})(y_1-x_1)d\mathbf{y}$, $\int_{(\Omega\cup\mathcal{B}\Omega)\cap\mathcal{H}(\mathbf{x},\delta)}(y_2-x_2)\gamma(\mathbf{x},\mathbf{y})(y_2-x_2)d\mathbf{y}$, and $\int_{(\Omega\cup\mathcal{B}\Omega)\cap\mathcal{H}(\mathbf{x},\delta)}(y_1-x_1)\gamma(\mathbf{x},\mathbf{y})(y_2-x_2)d\mathbf{y}$. Furthermore, for kernels $\gamma(\mathbf{x},\mathbf{y})$ of the types expressed in Eqs. (4) and (5), the functions in \mathbf{V}_h only depend on $\mathbf{y}-\mathbf{x}$, meaning that the quadrature weights depend only on the relative position between the quadrature points in $\{\mathbf{x}_{qp}^e\}_{p=1}^{Nqp}$ and the center of the ball \mathbf{x}_q^e , i.e., $\mathbf{x}_q^e-\mathbf{x}_q^e$, for arbitrary p,q. Since the positions of the points \mathbf{x}_q^e are defined relative to \mathbf{x}_q^e (see Eq. (43)), their relative positions with respect to the centers of the balls are always the same for all full balls. Therefore, the quadrature weights can be evaluated once for a representative full ball and used for all full balls $\mathcal{H}(\mathbf{x}_q^e,\delta)$, $\forall \mathbf{x}_q^e\in\Omega\cup\partial\Omega$.

Note that in [50] a similar placement of quadrature points within the full ball $\mathcal{H}(\mathbf{x}_q^e, \delta)$, i.e., quadrature points in a regular uniform grid, symmetrically distributed around \mathbf{x}_q^e , was employed for the numerical quadrature of strongform nonlocal diffusion. Furthermore, conditions for obtaining positive quadrature weights, as well as expressions for them, are also provided in [50]. While in this work we do not explicitly impose any restriction on the positivity of the weights, in all our tests the quadrature weights $\left\{\omega_{qp}^e\right\}_{p=1}^{N_{qp}}$ are verified to be positive.

Next, we consider the case in which $\mathbf{x}_q^e \in \mathcal{B}\Omega \setminus \partial\Omega$. In this case, $(\Omega \cup \mathcal{B}\Omega) \cap \mathcal{H}(\mathbf{x}_q^e, \delta) \subset \mathcal{H}(\mathbf{x}_q^e, \delta)$, i.e., the integration over $(\Omega \cup \mathcal{B}\Omega) \cap \mathcal{H}(\mathbf{x}_q^e, \delta)$ is over a *partial* or *truncated* ball (see Fig. 7 for an example of a two-dimensional partial Euclidean ball). Therefore, the set of points defined by Eq. (46) will not be symmetrical with respect to its associated \mathbf{x}_q^e . Moreover, its dimension N_{qp} will also be different depending on the position of \mathbf{x}_q^e . For this reason, a different set of weights $\{\omega_{qp}^e\}_{p=1}^{N_{qp}}$ needs to be computed $\forall q$ such that $\mathbf{x}_q^e \in (\mathcal{B}\Omega \setminus \partial\Omega)$. Recall that the expressions in Section 3 were presented for integrals over full balls. For partial balls, the constraints in the optimization problem in Eq. (25) can be stated as

$$\sum_{\substack{p=1\\p:\mathbf{X}_q^e,p\neq\mathbf{x}_q^e}}^{N_{qp}} f_j\omega_j = \int_{\mathscr{H}(\mathbf{x}_q^e,\delta)\cap(\Omega\cup\mathscr{B}\Omega)} f(\mathbf{x}_q^e,\mathbf{y})d\mathbf{y} \ \forall f\in\mathbf{V}_h.$$

$$\tag{49}$$

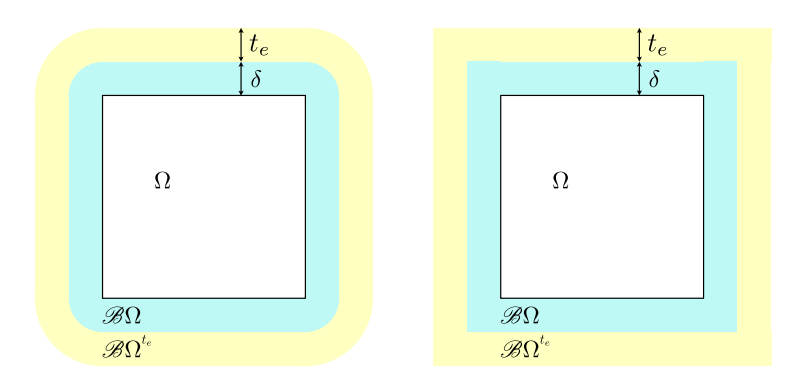


Fig. 5. Left: a square domain Ω (in white) with its corresponding interaction domain $\mathcal{B}\Omega$ (in light-blue) and its interaction domain extension $\mathcal{B}\Omega^{te}$ (in yellow). Right: the same square domain and polygonal approximate interaction domain and interaction domain extension, still referred to as $\mathcal{B}\Omega$ and $\mathcal{B}\Omega^{te}$, respectively. (For interpretation of the references to color in this figure legend, the reader is referred to the web version of this article.)

Due to the complex geometry of $\mathcal{H}(\mathbf{x}_q^e, \delta) \cap (\Omega \cup \mathcal{B}\Omega)$, the analytical integral on the right-hand side of Eq. (49) is particularly cumbersome. Therefore, in this work, we follow [32,46,50,51] and approximate the right-hand side of Eq. (49) with the integral over the full ball, as in Eq. (25).

4.2.1. Special treatment of the nonlocal boundary

Let us now consider $q_1 \in e_1$, and $q_2 \in e_2$ such that $\mathbf{x}_{q_1}^{e_1} \in \Omega \cup \partial \Omega$, and $\mathbf{x}_{q_2}^{e_2} \in \mathcal{B}\Omega \setminus \partial \Omega$, and two points $\mathbf{x}_{q_1p_i}^{e_1} \in \{\mathbf{x}_{q_1p}^{e_1}\}_{p=1}^{N_{q_1p}}$, and $\mathbf{x}_{q_2p_j}^{e_2} \in \{\mathbf{x}_{q_2p}^{e_2}\}_{p=1}^{N_{q_2p}}$, such that

$$\mathbf{x}_{q_1p_i}^{e_1} - \mathbf{x}_{q_1}^{e_1} = \mathbf{x}_{q_2p_i}^{e_2} - \mathbf{x}_{q_2}^{e_2}. \tag{50}$$

By employing the optimization-based procedure described in Section 3 with the finite-dimensional space in (48), we can determine the sets of weights $\{\omega_{q_1p}^{e_1}\}_{p=1}^{N_{q_1p}}$ and $\{\omega_{q_2p}^{e_2}\}_{p=1}^{N_{q_2p}}$ associated with $\{\mathbf{x}_{q_1p}^{e_1}\}_{p=1}^{N_{q_1p}}$ and $\mathbf{x}_{q_2p_j}^{e_2} \in \{\mathbf{x}_{q_2p}^{e_2}\}_{p=1}^{N_{q_2p}}$, respectively. In general, $\omega_{q_1p_i}^{e_1} \neq \omega_{q_2p_j}^{e_2}$, meaning that two quadrature points with the same relative position with respect to the center \mathbf{x}_q^e of the corresponding ball will have different weights. As illustrated numerically in Section 6.1.1, this fact may cause the discretization error to increase near the boundary $\mathcal{B}\Omega$. To circumvent this issue, we consider an extension of the interaction domain of size t_e , with $0 \leq t_e \leq \delta$, for the computation of the inner quadrature weights. To this end, we define

$$\mathscr{B}\Omega^{t_e} := \left\{ \mathbf{y} \in \mathbb{R}^d \setminus \Omega : \exists \mathbf{x} \in \Omega \text{ such that } |\mathbf{y} - \mathbf{x}|_{\ell^{\tilde{p}}} \le (\delta + t_e) \right\} \setminus \mathscr{B}\Omega. \tag{51}$$

As discussed above, for the interaction domain $\mathcal{B}\Omega$, in the case of Euclidean balls, i.e., $\tilde{p}=2$, $\mathcal{B}\Omega^{t_e}$ will have rounded corners, which we replace with vertices to make $\mathcal{B}\Omega^{t_e}$ a polyhedral domain that can be easily meshed (see Fig. 5 for a two-dimensional illustration).

Now, $\forall \mathbf{x}_q^e \in (\Omega \cup \mathcal{B}\Omega)$, we define the following set of points

$$\begin{aligned}
\left\{\mathbf{x}_{qp}^{e}\right\}_{p=1}^{\tilde{N}_{qp}} &:= \left\{\mathbf{x}_{qp}^{e}\right\}_{p=1}^{\overline{N}_{qp}} \cap \mathcal{H}(\mathbf{x}_{q}^{e}, \delta) \cap \left(\Omega \cup \mathcal{B}\Omega \cup \mathcal{B}\Omega^{te}\right) \\
&= \left\{\mathbf{x}_{qp}^{e} \in \left\{\mathbf{x}_{qp}^{e}\right\}_{p=1}^{\overline{N}_{qp}} \cap \left(\Omega \cup \mathcal{B}\Omega \cup \mathcal{B}\Omega^{te}\right) : |\mathbf{x}_{qp}^{e} - \mathbf{x}_{q}^{e}|_{\ell^{\tilde{p}}} \leq \delta\right\},
\end{aligned} (52)$$

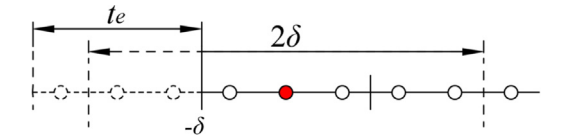


Fig. 6. One-dimensional partial integration ball for the filled red point and mesh extension of size t_e . The shown region is the left region of a domain $\mathcal{B}\Omega \cup \Omega = [-\delta, 1 + \delta]$, with $\Omega = (0, 1)$.

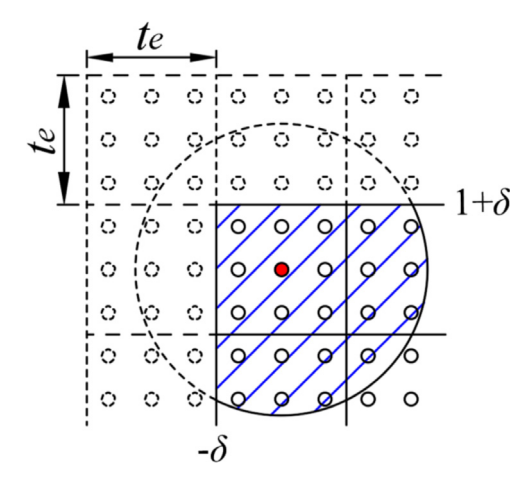


Fig. 7. Two-dimensional partial integration Euclidean ball for the filled red point (shaded area) and mesh extension of size t_e . The shown region is the top-left region of a domain $\mathcal{B}\Omega \cup \Omega = [-\delta, 1+\delta] \times [-\delta, 1+\delta]$, with $\Omega = (0,1) \times (0,1)$.

which coincides to the one defined in (46) for $t_e = 0$ and, regardless of t_e , $\forall \mathbf{x}_q^e \in (\Omega \cup \partial \Omega)$. For $t_e = \delta$, we have $(\Omega \cup \mathcal{B}\Omega \cup \mathcal{B}\Omega^{t_e}) \cap \mathcal{H}(\mathbf{x}_q^e, \delta) = \mathcal{H}(\mathbf{x}_q^e, \delta)$, meaning that for every $\mathbf{x}_q^e \in (\Omega \cup \mathcal{B}\Omega)$ the set of points defined in (52) is distributed across each full ball $\mathcal{H}(\mathbf{x}_q^e, \delta)$, as illustrated in Figs. 6 and 7 for a one-dimensional and a two-dimensional case, respectively.

We can now employ the optimization procedure from Section 3, for the finite dimensional space defined in (48), to determine the set of weights $\{\omega_{qp}^e\}_{p=1}^{\tilde{N}_{qp}}$. We can then select $\{\mathbf{x}_{qp}^e\}_{p=1}^{N_{qp}}\subseteq \{\mathbf{x}_{qp}^e\}_{p=1}^{\tilde{N}_{qp}}$ as

$$\left\{\mathbf{x}_{qp}^{e}\right\}_{p=1}^{N_{qp}} := \left\{\mathbf{x}_{qp}^{e} \in \left\{\mathbf{x}_{qp}^{e}\right\}_{p=1}^{\tilde{N}_{qp}} \cap (\Omega \cup \mathcal{B}\Omega)\right\},\tag{53}$$

and their associated weights $\left\{\omega_{qp}^e\right\}_{p=1}^{N_{qp}}\subseteq\left\{\omega_{qp}^e\right\}_{p=1}^{\tilde{N}_{qp}}$. Therefore, from Eqs. (41) and (42), we can obtain

$$D(w^{h}, v^{h}) \approx \sum_{\Omega_{e}^{h} \in \mathcal{M}^{h}} \sum_{q=1}^{N_{q}} \int_{(\Omega \cup \mathcal{B}\Omega) \cap \mathcal{H}(\mathbf{x}_{q}^{e}, \delta)} \left[v^{h}(\mathbf{y}) - v^{h}(\mathbf{x}_{q}^{e}) \right] \gamma(\mathbf{x}_{q}^{e}, \mathbf{y}) \left[w^{h}(\mathbf{y}) - w^{h}(\mathbf{x}_{q}^{e}) \right] d\mathbf{y} \omega_{q}^{e}$$

$$\approx \sum_{\Omega_{e}^{h} \in \mathcal{M}^{h}} \sum_{q=1}^{N_{q}} \sum_{p=1}^{N_{q}} \left[v^{h}(\mathbf{x}_{qp}^{e}) - v^{h}(\mathbf{x}_{q}^{e}) \right] \gamma(\mathbf{x}_{q}^{e}, \mathbf{x}_{qp}^{e}) \left[w^{h}(\mathbf{x}_{qp}^{e}) - w^{h}(\mathbf{x}_{q}^{e}) \right] \omega_{qp}^{e} \omega_{q}^{e}$$

$$= D^{h}(w^{h}, v^{h}),$$
(54)

and

$$G(v^{h}) - D(g^{h}, v^{h}) \approx \sum_{\Omega_{e}^{h} \in \mathcal{M}_{\Omega}^{h}} \sum_{b=1}^{N_{b}} v^{h}(\mathbf{x}_{b}^{e})b(\mathbf{x}_{b}^{e})\omega_{b}^{e}$$

$$- \sum_{\Omega_{e}^{h} \in \mathcal{M}^{h}} \sum_{q=1}^{N_{q}} \int_{(\Omega \cup \mathcal{B}\Omega) \cap \mathcal{H}(\mathbf{x}_{q}^{e}, \delta)} \left[v^{h}(\mathbf{y}) - v^{h}(\mathbf{x}_{q}^{e}) \right] \gamma(\mathbf{x}_{q}^{e}, \mathbf{y}) \left[g^{h}(\mathbf{y}) - g^{h}(\mathbf{x}_{q}^{e}) \right] d\mathbf{y}\omega_{q}^{e}$$

$$\approx \sum_{\Omega_{e}^{h} \in \mathcal{M}_{\Omega}^{h}} \sum_{b=1}^{N_{b}} v^{h}(\mathbf{x}_{b}^{e})b(\mathbf{x}_{b}^{e})\omega_{b}^{e}$$

$$- \sum_{\Omega_{e}^{h} \in \mathcal{M}^{h}} \sum_{q=1}^{N_{q}} \sum_{p=1}^{N_{q}} \left[v^{h}(\mathbf{x}_{qp}^{e}) - v^{h}(\mathbf{x}_{q}^{e}) \right] \gamma(\mathbf{x}_{q}^{e}, \mathbf{x}_{qp}^{e}) \left[g^{h}(\mathbf{x}_{qp}^{e}) - g^{h}(\mathbf{x}_{q}^{e}) \right] \omega_{qp}^{e}\omega_{q}^{e}$$

$$= G^{h}(v^{h}) - D^{h}(g^{h}, v^{h}),$$

$$(55)$$

where we defined

$$D^{h}(\cdot, v^{h}) := \sum_{Q^{h} \in \mathcal{M}^{h}} \sum_{q=1}^{N_{qp}} \sum_{p=1}^{N_{qp}} \left[v^{h}(\mathbf{x}_{qp}^{e}) - v^{h}(\mathbf{x}_{q}^{e}) \right] \gamma(\mathbf{x}_{q}^{e}, \mathbf{x}_{qp}^{e}) \left[(\cdot)(\mathbf{x}_{qp}^{e}) - (\cdot)(\mathbf{x}_{q}^{e}) \right] \omega_{qp}^{e} \omega_{q}^{e}, \tag{56}$$

and

$$G^{h}(v^{h}) := \sum_{\Omega_{e}^{h} \in \mathcal{M}_{Q}^{h}} \sum_{b=1}^{N_{b}} v^{h}(\mathbf{x}_{b}^{e}) b(\mathbf{x}_{b}^{e}) \omega_{b}^{e}. \tag{57}$$

4.3. Fully discrete variational form for nonlocal diffusion

We combine the finite element discretization from Section 4.1 with the discrete quadrature approach discussed in Section 4.2. By substituting the continuous operators in (34) with the discrete ones defined in Eqs. (56) and (57), we get

$$D^{h}(w^{h}, v^{h}) = G^{h}(v^{h}) - D^{h}(g^{h}, v^{h}), \tag{58}$$

which, by employing Eqs. (30) and (32), results in the following linear system

$$\sum_{i=1}^{J_{\Omega}} D^h(\psi_j, \psi_i) u_j = G^h(\psi_i) - D^h(g^h, \psi_i), \tag{59}$$

for $i = 1, ..., J_{\Omega}$. Eq. (59) can be expressed in matrix form as

$$\mathbf{A}^h \mathbf{u} = \mathbf{f}^h, \tag{60}$$

where \mathbf{A}^h is a $J_{\Omega} \times J_{\Omega}$ matrix with components

$$A_{ij}^{h} = D^{h}(\psi_{j}, \psi_{i})$$

$$= \sum_{\Omega_{r}^{h} \in \mathcal{M}^{h}} \sum_{q=1}^{N_{q}} \sum_{p=1}^{N_{qp}} \left[\psi_{i}(\mathbf{x}_{qp}^{e}) - \psi_{i}(\mathbf{x}_{q}^{e}) \right] \gamma(\mathbf{x}_{q}^{e}, \mathbf{x}_{qp}^{e}) \left[\psi_{j}(\mathbf{x}_{qp}^{e}) - \psi_{j}(\mathbf{x}_{q}^{e}) \right] \omega_{qp}^{e} \omega_{q}^{e},$$

$$(61)$$

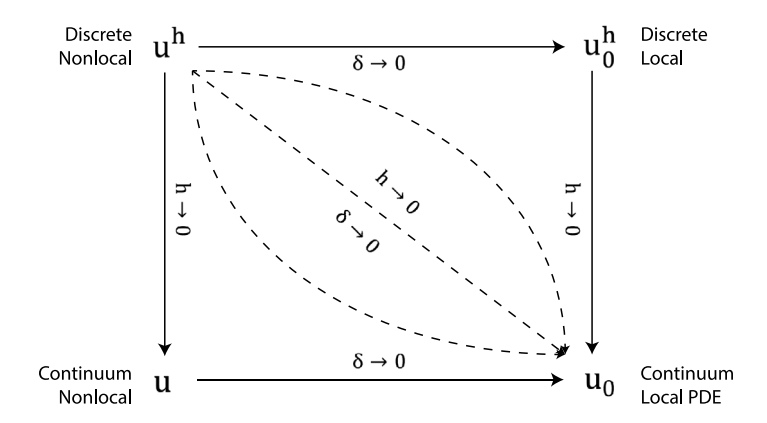


Fig. 8. Different convergence paths in finite-length nonlocal model. u and u_0 represent the continuum nonlocal and local solutions, respectively, while u^h and u^h_0 are their discrete counterparts.

 \mathbf{f}^h is a $J_{\Omega} \times 1$ vector with components

$$f_{i}^{h} = G^{h}(\psi_{i}) - D^{h}(g^{h}, \psi_{i}) = \sum_{\Omega_{e}^{h} \in \mathcal{M}_{\Omega}^{h}} \sum_{b=1}^{N_{b}} \psi_{i}(\mathbf{x}_{b}^{e}) b(\mathbf{x}_{b}^{e}) \omega_{b}^{e}$$

$$- \sum_{\Omega_{e}^{h} \in \mathcal{M}^{h}} \sum_{q=1}^{N_{q}} \sum_{p=1}^{N_{qp}} \left[\psi_{i}(\mathbf{x}_{qp}^{e}) - \psi_{i}(\mathbf{x}_{q}^{e}) \right] \gamma(\mathbf{x}_{q}^{e}, \mathbf{x}_{qp}^{e}) \left[g^{h}(\mathbf{x}_{qp}^{e}) - g^{h}(\mathbf{x}_{q}^{e}) \right] \omega_{qp}^{e} \omega_{q}^{e},$$

$$(62)$$

and **u** is a vector of size $J_{\Omega} \times 1$ containing the set of unknown coefficients $\{u_i\}_{i=1}^{J_{\Omega}}$ to be determined.

5. Properties of the numerical scheme

In this section, we investigate the numerical properties of the proposed scheme. We first describe different types of convergence in the context of nonlocal models (see Fig. 8) and then provide a convergence analysis in the H^1 norm in a simplified, one-dimensional setting.

5.1. Brief review of asymptotically compatible schemes

As described in Section 2, continuum nonlocal models are characterized by the length scale δ . Under proper regularity assumptions, as $\delta \to 0$, nonlocal solutions converge to their local, PDE counterparts [63]; we refer to this type of convergence as δ -convergence. When a discretization scheme is employed, its size h introduces a second length scale. For a fixed horizon δ , a discretization scheme is h-convergent if the nonlocal discrete solution converges to the continuum nonlocal solution as $h \to 0$. Lastly, a discretization scheme is called *asymptotically compatible* if, in addition to the δ - and h-convergence above, the discrete solution to the nonlocal problem also converges to the analytical solution of its local PDE counterpart as $\delta \to 0$ and $h \to 0$ [64,65]. For numerical schemes where h and δ are tied together by the relationship $m = \delta/h$, the term *asymptotic compatibility* refers only to the last type of convergence described above, i.e., meaning that as $\delta \to 0$ and $h \to 0$, the discrete solution to the nonlocal problem converges to the analytical solution of the associated local problem [46,50]. As the proposed scheme is such that $m = \delta/h \in \mathbb{N}$, we will only focus on the latter type of convergence (i.e., $\delta \to 0$ and $h \to 0$ simultaneously).

5.2. Convergence analysis

In this section we derive a preliminary estimate for the convergence of discrete solutions obtained via inexact quadrature of the inner integral. We assume that the outer quadrature is performed with a high-accuracy scheme

whose contribution to the overall error can be considered negligible. In the following analysis we hence assume the outer integration to be exact. Therefore,

$$D^{h}(u^{h}, u^{h}) = \int_{\Omega \cup \mathcal{B}\Omega} \sum_{j=1}^{N_{j}} \gamma(\mathbf{x}, \mathbf{x}_{j}) \left[u^{h}(\mathbf{x}_{j}) - u^{h}(\mathbf{x}) \right]^{2} \omega_{j} d\mathbf{x}$$

$$= \sum_{\Omega_{e}^{h} \in \mathcal{M}^{h}} \int_{\Omega_{e}^{h}} \sum_{j=1}^{N_{j}} \gamma(\mathbf{x}, \mathbf{x}_{j}) \left[u^{h}(\mathbf{x}_{j}) - u^{h}(\mathbf{x}) \right]^{2} \omega_{j} d\mathbf{x},$$
(63)

where \mathbf{x}_j and ω_j are the jth inner quadrature point and associated weight in the ball $\mathcal{H}(\mathbf{x}, \delta)$, respectively, and N_j is the total number of inner quadrature points. Furthermore, we also restrict ourselves to kernels of the form (4).

5.2.1. Uniform V^h -coercivity

We show, under certain conditions, that the approximate bilinear form $D^h(\cdot, \cdot): \mathcal{V}^h \times \mathcal{V}^h \to \mathbb{R}$ is uniformly \mathcal{V}^h -coercive. Recall that we are considering a C^0 linear FE approximation. Therefore, $\forall \mathbf{x}$

$$u^{h}(\mathbf{x}_{j}) - u^{h}(\mathbf{x}) = \begin{cases} \nabla u^{h}(\mathbf{x})|_{e} \cdot (\mathbf{x}_{j} - \mathbf{x}), & \text{for } \mathbf{x}_{j}, \mathbf{x} \text{ in element } e, \\ u^{h}(\mathbf{x}_{j}) - u^{h}(\mathbf{x}), & \text{otherwise.} \end{cases}$$
(64)

We assume that we have a subset of the quadrature points $\{\mathbf{x}_j\}$ that are in the same element as \mathbf{x} , $\{\mathbf{x}_{j_{\text{in}}}\}$, and another subset of the quadrature points that are not, $\{\mathbf{x}_{j_{\text{out}}}\}$. Membership of points in these subsets is linked to the chosen spacing for the quadrature points; we assume that this spacing is small enough relative to the element size so that $\{\mathbf{x}_{j_{\text{in}}}\}$ is nonempty. We also assume that the inner quadrature weights $\{\omega_j\}$ are positive. Then, Eq. (63) can be recast as

$$D^{h}(u^{h}, u^{h}) = \sum_{\Omega_{e}^{h} \in \mathcal{M}^{h}} \int_{\Omega_{e}^{h}} \left[\sum_{j_{\text{in}}=1}^{N_{j_{\text{in}}}} \gamma(\mathbf{x}, \mathbf{x}_{j_{\text{in}}}) \left[u^{h}(\mathbf{x}_{j_{\text{in}}}) - u^{h}(\mathbf{x}) \right]^{2} \omega_{j_{\text{in}}} \right.$$

$$\left. + \sum_{j_{\text{out}}=1}^{N_{j_{\text{out}}}} \gamma(\mathbf{x}, \mathbf{x}_{j_{\text{out}}}) \left[u^{h}(\mathbf{x}_{j_{\text{out}}}) - u^{h}(\mathbf{x}) \right]^{2} \omega_{j_{\text{out}}} \right] d\mathbf{x}$$

$$\geq \sum_{\Omega_{e}^{h} \in \mathcal{M}^{h}} \int_{\Omega_{e}^{h}} \sum_{j_{\text{in}}=1}^{N_{j_{\text{in}}}} \gamma(\mathbf{x}, \mathbf{x}_{j_{\text{in}}}) \left[u^{h}(\mathbf{x}_{j_{\text{in}}}) - u^{h}(\mathbf{x}) \right]^{2} \omega_{j_{\text{in}}} d\mathbf{x}.$$

$$(65)$$

We first consider the constant kernel in Eq. (4). Eq. (65) then becomes

$$D^{h}(u^{h}, u^{h}) \geq \sum_{\Omega_{e}^{h} \in \mathcal{M}^{h}} \int_{\Omega_{e}^{h}} \sum_{j_{\text{in}}=1}^{N_{j_{\text{in}}}} \gamma(\mathbf{x}, \mathbf{x}_{j_{\text{in}}}) \left[u^{h}(\mathbf{x}_{j_{\text{in}}}) - u^{h}(\mathbf{x}) \right]^{2} \omega_{j_{\text{in}}} d\mathbf{x}$$

$$= \frac{\zeta_{c}}{\delta^{d+2}} \sum_{\Omega_{e}^{h} \in \mathcal{M}^{h}} \int_{\Omega_{e}^{h}} \sum_{j_{\text{in}}=1}^{N_{j_{\text{in}}}} \left[u^{h}(\mathbf{x}_{j_{\text{in}}}) - u^{h}(\mathbf{x}) \right]^{2} \omega_{j_{\text{in}}} d\mathbf{x}.$$

$$(66)$$

If, instead, the kernel is of the type from Eq. (5) with $\tilde{p}=2$, Eq. (65) becomes

$$D^{h}(u^{h}, u^{h}) \geq \sum_{\Omega_{e}^{h} \in \mathcal{M}^{h}} \int_{\Omega_{e}^{h}} \sum_{j_{\text{in}}=1}^{N_{j_{\text{in}}}} \gamma(\mathbf{x}, \mathbf{x}_{j_{\text{in}}}) \left[u^{h}(\mathbf{x}_{j_{\text{in}}}) - u^{h}(\mathbf{x}) \right]^{2} \omega_{j_{\text{in}}} d\mathbf{x}$$

$$= \frac{\zeta_{r}}{\delta^{d+1}} \sum_{\Omega_{e}^{h} \in \mathcal{M}^{h}} \int_{\Omega_{e}^{h}} \sum_{j_{\text{in}}=1}^{N_{j_{\text{in}}}} \frac{1}{|\mathbf{x}_{j_{\text{in}}} - \mathbf{x}|_{\ell^{2}}} \left[u^{h}(\mathbf{x}_{j_{\text{in}}}) - u^{h}(\mathbf{x}) \right]^{2} \omega_{j_{\text{in}}} d\mathbf{x}$$

$$\geq \frac{\zeta_{r}}{\delta^{d+2}} \sum_{\Omega_{e}^{h} \in \mathcal{M}^{h}} \int_{\Omega_{e}^{h}} \sum_{j_{\text{in}}=1}^{N_{j_{\text{in}}}} \left[u^{h}(\mathbf{x}_{j_{\text{in}}}) - u^{h}(\mathbf{x}) \right]^{2} \omega_{j_{\text{in}}} d\mathbf{x}.$$

$$(67)$$

By comparing Eqs. (66) and (67), we see that for both kernel we have a similar expression for the lower bound, which we can express by dropping the subscript in the ζ -terms as

$$D^{h}(u^{h}, u^{h}) \geq \frac{\zeta}{\delta^{d+2}} \sum_{\Omega_{e}^{h} \in \mathcal{M}^{h}} \int_{\Omega_{e}^{h}} \sum_{j_{\text{in}}=1}^{N_{j_{\text{in}}}} \left[u^{h}(\mathbf{x}_{j_{\text{in}}}) - u^{h}(\mathbf{x}) \right]^{2} \omega_{j_{\text{in}}} d\mathbf{x}$$

$$= \frac{\zeta}{\delta^{d+2}} \sum_{\Omega_{e}^{h} \in \mathcal{M}^{h}} \int_{\Omega_{e}^{h}} \sum_{j_{\text{in}}=1}^{N_{j_{\text{in}}}} \left[\left. \nabla u^{h}(\mathbf{x}) \right|_{e} \cdot (\mathbf{x}_{j_{\text{in}}} - \mathbf{x}) \right]^{2} \omega_{j_{\text{in}}} d\mathbf{x}.$$

$$(68)$$

For simplicity, we now restrict our discussion to the one-dimensional case. In this setting, we assume that there exists a constant C > 0 independent of h and δ , such that $C\delta < \omega_{\min} < \omega_{j_{\text{in}}}$ (which we verify by direct computation in A). Under these assumptions, we have the following coercivity result for the discrete bilinear form.

Lemma 5.1. There exists a constant c > 0 independent of h and δ such that $\forall u^h \in \mathcal{V}_0^h$

$$D^{h}(u^{h}, u^{h}) \ge c|u^{h}|_{H^{1}}^{2}. \tag{69}$$

Proof. Restricting Eq. (68) to the one-dimensional setting, using our assumed lower bound on $\omega_{j_{\rm in}}$, abbreviating restriction of u^h to element e as u_e^h , and allowing the symbol C to be a generic constant independent of h and δ (possibly with different numerical values in different places), we get

$$\begin{split} D^h(u^h, u^h) &\geq \frac{\zeta}{\delta^3} \sum_{\Omega_e^h \in \mathcal{M}^h} \int_{\Omega_e^h} \sum_{j_{\text{in}}=1}^{N_{j_{\text{in}}}} \left[u^h(x_{j_{\text{in}}}) - u^h(x) \right]^2 \omega_{j_{\text{in}}} dx \\ &= \frac{\zeta}{\delta^3} \sum_{\Omega_e^h \in \mathcal{M}^h} \int_{\Omega_e^h} \left[\sum_{j_{\text{in}}=1}^{N_{j_{\text{in}}}} \left\{ \frac{du_e^h}{dx} \cdot (x_{j_{\text{in}}} - x) \right\}^2 \omega_{j_{\text{in}}} \right] dx \\ &= \frac{\zeta}{\delta^3} \sum_{\Omega_e^h \in \mathcal{M}^h} \left(\frac{du_e^h}{dx} \right)^2 \int_{\Omega_e^h} \left[\sum_{j_{\text{in}}=1}^{N_{j_{\text{in}}}} (x_{j_{\text{in}}} - x)^2 \omega_{j_{\text{in}}} \right] dx \\ &= \frac{\zeta}{\delta^3} \sum_{\Omega_e^h \in \mathcal{M}^h} \left(\frac{du_e^h}{dx} \right)^2 \sum_{j_{\text{in}}=1}^{N_{j_{\text{in}}}} \left\{ \int_{\Omega_e^h \setminus (x_{j_{\text{in}}} - h/4, x_{j_{\text{in}}} + h/4)} (x_{j_{\text{in}}} - x)^2 \omega_{j_{\text{in}}} dx \right\} \\ &\geq \frac{\zeta}{\delta^3} \sum_{\Omega_e^h \in \mathcal{M}^h} \left(\frac{du_e^h}{dx} \right)^2 \sum_{j_{\text{in}}=1}^{N_{j_{\text{in}}}} \left\{ \int_{\Omega_e^h \setminus (x_{j_{\text{in}}} - h/4, x_{j_{\text{in}}} + h/4)} (x_{j_{\text{in}}} - x)^2 \omega_{j_{\text{in}}} dx \right\} \\ &\geq \frac{\zeta}{\delta^3} \sum_{\Omega_e^h \in \mathcal{M}^h} \left(\frac{du_e^h}{dx} \right)^2 \sum_{j_{\text{in}}=1}^{N_{j_{\text{in}}}} \left\{ \left(\frac{h}{2} \right) \left(\frac{h}{4} \right)^2 \omega_{j_{\text{in}}} \right\} \\ &\geq \frac{\zeta}{\delta^3} \sum_{\Omega_e^h \in \mathcal{M}^h} \left(\frac{du_e^h}{dx} \right)^2 \left\{ Ch^3 \omega_{\text{min}} \right\} \\ &\geq \frac{\zeta}{\delta^3} \sum_{\Omega_e^h \in \mathcal{M}^h} \left(\frac{du_e^h}{dx} \right)^2 \left\{ Ch^3 \omega_{\text{min}} \right\} \\ &\geq \frac{\zeta}{\delta^3} \sum_{\Omega_e^h \in \mathcal{M}^h} \left(\frac{du_e^h}{dx} \right)^2 \left\{ Ch^3 \delta \right\} \end{split}$$

$$\geq \frac{C}{\delta^3} \left(\sum_{\Omega_e^h \in \mathcal{M}^h} \left(\frac{du_e^h}{dx} \right)^2 h \right) h^2 \delta$$

$$\geq \frac{Ch^2}{\delta^2} |u^h|_{H^1}^2, \tag{70}$$

which gives the desired result when $h \sim \delta$.

5.2.2. Preliminary convergence estimate

We prove the convergence of numerical solutions for a simple one-dimensional case with a uniform grid and $\delta = h$. To do that, we first prove a lemma that holds in more general situations. We assume that for any $v^h \in \mathcal{V}_0^h$, $\int b(\mathbf{x}) v^h(\mathbf{x}) d\mathbf{x}$ is exactly integrated. By using the same arguments as in Strang's first lemma, we have the following result.

Lemma 5.2. There exists C > 0 independent of δ such that

$$\|u-u^h\|_{\mathcal{V}} \le C \inf_{v^h \in \mathcal{V}_0^h} \left(\|u-v^h\|_{\mathcal{V}} + \sup_{w^h \in \mathcal{V}_0^h} \frac{|D(v^h, w^h) - D^h(v^h, w^h)|}{\|w^h\|_{\mathcal{V}}} \right).$$

In addition, if $u \in H^1$, then

$$||u - u^h||_{H^1} \le C \inf_{v^h \in \mathcal{V}_0^h} \left(||u - v^h||_{H^1} + \sup_{w^h \in \mathcal{V}_0^h} \frac{|D(v^h, w^h) - D^h(v^h, w^h)|}{||w^h||_{\mathcal{V}}} \right)$$

Proof. By Lemma 5.1, for any $v^h \in \mathcal{V}_0^h$, we have

$$\begin{split} c|u^h - v^h|_{H^1}^2 &\leq D^h(u^h - v^h, u^h - v^h) \\ &= D(u - v^h, u^h - v^h) + (D(v^h, u^h - v^h) - D^h(v^h, u^h - v^h)) \\ &+ (D^h(u^h, u^h - v^h) - D(u, u^h - v^h)) \\ &= D(u - v^h, u^h - v^h) + (D(v^h, u^h - v^h) - D^h(v^h, u^h - v^h)). \end{split}$$

By the boundedness of the bilinear form, i.e., $|D(u-v^h,u^h-v^h)| \leq C||u-v^h||_{\mathcal{V}}||u^h-v^h||_{\mathcal{V}}$, where we write $||w||_{\mathcal{V}} = \sqrt{D(w,w)}$ for $w \in \mathcal{V}$, we have

$$c\frac{|u^{h}-v^{h}|_{H^{1}}^{2}}{\|u^{h}-v^{h}\|_{\mathcal{V}}^{2}} \leq C\|u-v^{h}\|_{\mathcal{V}} + \frac{|D(v^{h},u^{h}-v^{h})-D^{h}(v^{h},u^{h}-v^{h})|}{\|u^{h}-v^{h}\|_{\mathcal{V}}}$$

$$\leq C\|u-v^{h}\|_{\mathcal{V}} + \sup_{w^{h}\in\mathcal{V}_{0}^{h}} \frac{|D(v^{h},w^{h})-D^{h}(v^{h},w^{h})|}{\|w^{h}\|_{\mathcal{V}}}.$$

$$(71)$$

Notice that H^1 is continuously embedded in \mathcal{V} , i.e.,

$$||v||_{\mathcal{V}} < C||v||_{H^1} \quad \forall v \in H^1,$$

where the constant C is independent of δ (see e.g., [66]). From (71), for any $v^h \in \mathcal{V}_0^h$

$$\|u^h - v^h\|_{\mathcal{V}} \le C \left(\|u - v^h\|_{\mathcal{V}} + \sup_{w^h \in \mathcal{V}_0^h} \frac{|D(v^h, w^h) - D^h(v^h, w^h)|}{\|w^h\|_{\mathcal{V}}} \right)$$

and, if in addition $u \in H^1$,

$$\|u^h - v^h\|_{H^1} \le C \left(\|u - v^h\|_{H^1} + \sup_{w^h \in \mathcal{V}_0^h} \frac{|D(v^h, w^h) - D^h(v^h, w^h)|}{\|w^h\|_{\mathcal{V}}} \right).$$

Therefore from the triangle inequality

$$||u - u^h|| < ||u - v^h|| + ||u^h - v^h||$$

with either the V-norm or the H^1 -norm, we can get the desired result. \square

The following theorem provides a convergence result for the simple one-dimensional case with a uniform grid, $\delta = h$ and a kernel function $\gamma(x, y) = \frac{1}{s3} \mathbf{1}_{\{|y-x|<\delta\}}$, where, for simplicity, we removed the constant ζ .

Theorem 5.3. Assume we have a uniform grid in one-dimension and $\delta = h$. In addition, assume that $u \in H^2$. Then,

$$||u - u^h||_{H^1} < Ch$$
,

where C > 0 is a constant that depends on $||u||_{H^2}$, but is independent of h and δ .

Proof. By Lemma 5.2 and $u \in H^2$, we have

$$\|u - u^h\|_{H^1} \le C \inf_{v^h \in \mathcal{V}_0^h} \left(\|u - v^h\|_{H^1} + \sup_{w^h \in \mathcal{V}_0^h} \frac{|D(v^h, w^h) - D^h(v^h, w^h)|}{\|w^h\|_{\mathcal{V}}} \right)$$

where, from Eq. (29), V_0^h is the space of continuous piecewise linear functions that satisfy zero Dirichlet boundary conditions. Taking $v^h := I_h u$, the piecewise linear interpolation of u, then it is well-known in finite element analysis that

$$||u - I_h u||_{H^1} \le Ch ||u||_{H^2}.$$

Let $\Omega \cup \mathcal{B}\Omega = \bigcup_{i=1}^N \Omega_i^h$ and extend functions by zero outside $\Omega \cup \mathcal{B}\Omega$ when necessary (e.g., on $\mathcal{B}\Omega^{t_e}$). Then, by assuming $\delta = h$, we have

$$D(v^{h}, w^{h}) = \sum_{i=1}^{N} \int_{\Omega_{i}^{h}} \int_{\mathcal{H}(x,\delta)} \gamma(x, y) (v^{h}(y) - v^{h}(x)) (w^{h}(y) - w^{h}(x)) dy dx$$

$$= \sum_{i=1}^{N} \int_{\Omega_{i}^{h}} \int_{\Omega_{i-1}^{h} \cup \Omega_{i}^{h} \cup \Omega_{i+1}^{h}} \gamma(x, y) (v^{h}(y) - v^{h}(x)) (w^{h}(y) - w^{h}(x)) dy dx.$$
(72)

Notice that in the above equation, Ω_0^h and Ω_{N+1}^h are outside $\Omega \cup \mathcal{B}\Omega$. Since the functions are always zero on Ω_0^h , Ω_1^h , Ω_N^h , Ω_{N+1}^h , we see that $\int_{\Omega_1^h} \int_{\Omega_0^h} \cdots$ and $\int_{\Omega_N^h} \int_{\Omega_{N+1}^h} \cdots$ are zero. Assume that on each Ω_i^h , $v^h(x)$ is a linear function of slope $a_i \in \mathbb{R}$, and $w^h(x)$ is a linear function of slope $b_i \in \mathbb{R}$, then we have

$$\int_{\Omega_{i}^{h}} \int_{\Omega_{i}^{h}} \gamma(x, y) (v^{h}(y) - v^{h}(x)) (w^{h}(y) - w^{h}(x)) dy dx = \int_{\Omega_{i}^{h}} \int_{\Omega_{i}^{h}} \gamma(x, y) (y - x)^{2} a_{i} b_{i} dy dx.$$
 (73)

Now we calculate $\int_{\Omega_i^h} \int_{\Omega_{i+1}^h} \cdots dy dx$. In this case, we have $y \in \Omega_{i+1}^h$ and $x \in \Omega_i^h$. Let s_i denote the point that connects Ω_i^h and Ω_{i+1}^h , then we can write

$$v^{h}(y) = v^{h}(s_{i}) + (y - s_{i})a_{i+1}, \quad w^{h}(y) = w^{h}(s_{i}) + (y - s_{i})b_{i+1},$$

$$v^{h}(x) = v^{h}(s_{i}) + (x - s_{i})a_{i}, \quad w^{h}(x) = w^{h}(s_{i}) + (x - s_{i})b_{i},$$
(74)

for all $y \in \Omega_{i+1}^h$ and $x \in \Omega_i^h$. Therefore,

$$v^{h}(y) - v^{h}(x) = (y - s_{i})a_{i+1} + (s_{i} - x)a_{i} = (y - s_{i})(a_{i+1} - a_{i}) + (y - x)a_{i}$$

$$(75)$$

and similarly for $w^h(y) - w^h(x)$. We then have

$$\int_{\Omega_{i}^{h}} \int_{\Omega_{i+1}^{h}} \gamma(x, y) (v^{h}(y) - v^{h}(x)) (w^{h}(y) - w^{h}(x)) dy dx
= \int_{\Omega_{i}^{h}} \int_{\Omega_{i+1}^{h}} \gamma(x, y) \left[(y - s_{i})(a_{i+1} - a_{i}) + (y - x)a_{i} \right] \left[(y - s_{i})(b_{i+1} - b_{i}) + (y - x)b_{i} \right] dy dx.$$
(76)

Notice that, in the above, there is a term $\int_{\Omega_i^h} \int_{\Omega_{i+1}^h} \gamma(x,y)(y-x)^2 a_i b_i dy dx$ which can be combined with $\int_{\Omega_i^h} \int_{\Omega_i^h} \gamma(x,y)(y-x)^2 a_i b_i dy dx$. The rest of the terms can be written as

$$\int_{\Omega_{i}^{h}} \int_{\Omega_{i+1}^{h}} \gamma(x, y) \left((y - s_{i})^{2} (a_{i+1} - a_{i})(b_{i+1} - b_{i}) + (y - s_{i})(y - x) \left[(a_{i+1} - a_{i})b_{i} + (b_{i+1} - b_{i})a_{i} \right] \right) dy dx
= \int_{\Omega_{i}^{h}} \int_{\Omega_{i+1}^{h}} \gamma(x, y) \left((y - s_{i})^{2} (a_{i+1}b_{i+1} - a_{i}b_{i}) + (y - s_{i})(s_{i} - x) \left[(a_{i+1} - a_{i})b_{i} + (b_{i+1} - b_{i})a_{i} \right] \right) dy dx
= (a_{i+1}b_{i+1} - a_{i}b_{i}) \int_{\Omega_{i}^{h}} \int_{s_{i}}^{x+\delta} \frac{(y - s_{i})^{2}}{\delta^{3}} dy dx
+ \left[(a_{i+1} - a_{i})b_{i} + (b_{i+1} - b_{i})a_{i} \right] \int_{\Omega_{i}^{h}} \int_{s_{i}}^{x+\delta} \frac{(y - s_{i})(s_{i} - x)}{\delta^{3}} dy dx.$$
(77)

We can similarly calculate $\int_{\Omega_i^h} \int_{\Omega_{i-1}^h} \cdots dy dx$ and get $\int_{\Omega_i^h} \int_{\Omega_{i-1}^h} \gamma(x,y) (y-x)^2 a_i b_i dy dx$ (which is to be combined with $\int_{\Omega_i^h} \int_{\Omega_i^h} \gamma(x,y) (y-x)^2 a_i b_i dy dx$) and

$$(a_{i-1}b_{i-1} - a_ib_i) \int_{\Omega_i^h} \int_{x-\delta}^{s_{i-1}} \frac{(y - s_{i-1})^2}{\delta^3} dy dx + [(a_{i-1} - a_i)b_i + (b_{i-1} - b_i)a_i] \int_{\Omega_i^h} \int_{x-\delta}^{s_{i-1}} \frac{(y - s_{i-1})(s_{i-1} - x)}{\delta^3} dy dx.$$

$$(78)$$

Replacing i-1 with i in (78), we get the contribution from $\int_{\Omega_{i+1}^h} \int_{\Omega_i^h} \cdots dy dx$:

$$(a_{i}b_{i} - a_{i+1}b_{i+1}) \int_{\Omega_{i+1}^{h}} \int_{x-\delta}^{s_{i}} \frac{(y-s_{i})^{2}}{\delta^{3}} dy dx$$

$$+ \left[(a_{i} - a_{i+1})b_{i+1} + (b_{i} - b_{i+1})a_{i+1} \right] \int_{\Omega_{i+1}^{h}} \int_{x-\delta}^{s_{i}} \frac{(y-s_{i})(s_{i}-x)}{\delta^{3}} dy dx$$

$$(79)$$

Now by adding (77) with (79) and noticing, from symmetry, that

$$\int_{\Omega_{i}^{h}} \int_{s_{i}}^{x+\delta} \frac{(y-s_{i})^{2}}{\delta^{3}} dy dx = \int_{\Omega_{i+1}^{h}} \int_{x-\delta}^{s_{i}} \frac{(y-s_{i})^{2}}{\delta^{3}} dy dx
\int_{\Omega_{i}^{h}} \int_{s_{i}}^{x+\delta} \frac{(y-s_{i})(s_{i}-x)}{\delta^{3}} dy dx = \int_{\Omega_{i+1}^{h}} \int_{x-\delta}^{s_{i}} \frac{(y-s_{i})(s_{i}-x)}{\delta^{3}} dy dx,$$
(80)

we get

$$|(77) + (79)| \le 2|a_{i+1} - a_i||b_{i+1} - b_i| \int_{\Omega_i^h} \int_{s_i}^{x+\delta} \frac{|y - s_i||s_i - x|}{\delta^3} dy dx$$

$$\le Ch|a_{i+1} - a_i||b_{i+1} - b_i|.$$
(81)

Combining the above results, we have

$$D(v^h, w^h) = \sum_{i=1}^{N} \int_{\Omega_i^h} \int_{\mathcal{H}(x,\delta)} \gamma(x, y) (y - x)^2 a_i b_i dy dx + \sum_{i=0}^{N} |a_{i+1} - a_i| |b_{i+1} - b_i| O(h).$$
 (82)

Now to estimate $D^h(v^h, w^h)$, we follow the exact procedure for $D(v^h, w^h)$, but with the inner integral replaced by GMLS quadrature. In particular, if we have symmetry of the quadrature points, then

$$\int_{\Omega_{i}^{h}} \sum_{s_{i} < y_{j} < x + \delta} \frac{(y_{j} - s_{i})^{2}}{\delta^{3}} \omega_{j} dx = \int_{\Omega_{i+1}^{h}} \sum_{x - \delta < y_{j} < s_{i}} \frac{(y_{j} - s_{i})^{2}}{\delta^{3}} \omega_{j} dx
\int_{\Omega_{i}^{h}} \sum_{s_{i} < y_{j} < x + \delta} \frac{(y_{j} - s_{i})(s_{i} - x)}{\delta^{3}} \omega_{j} dx = \int_{\Omega_{i+1}^{h}} \sum_{x - \delta < y_{j} < s_{i}} \frac{(y_{j} - s_{i})(s_{i} - x)}{\delta^{3}} \omega_{j} dx.$$
(83)

Then we can show that

$$D^{h}(v^{h}, w^{h}) = \sum_{i=1}^{N} \int_{\Omega_{i}^{h}} \sum_{i=1}^{NP} \gamma(x, y_{j})(y_{j} - x)^{2} a_{i} b_{i} \omega_{j} dx + \sum_{i=0}^{N} |a_{i+1} - a_{i}| |b_{i+1} - b_{i}| O(h).$$
(84)

Comparing (82) with (84), we notice that $\int_{\Omega_i^h} \int_{\mathscr{H}(x,\delta)} \gamma(x,y) (y-x)^2 dy dx = \int_{\Omega_i^h} \sum_{j=1}^{NP} \gamma(x,y_j) (y_j-x)^2 \omega_j dx$. We therefore only need an estimate of

$$\sup_{w^h \in \mathcal{V}_0^h} \frac{\sum_{i=0}^N |a_{i+1} - a_i| |b_{i+1} - b_i| O(h)}{\|w^h\|_{\mathcal{V}}}$$
(85)

with $v^h = I_h u$. Notice that $||w^h||_{\mathcal{V}} = \sqrt{D(w^h, w^h)}$, so we can write it out by the same procedure above and get

$$||w^{h}||_{\mathcal{V}}^{2} = \sum_{i=1}^{N} \int_{\Omega_{i}^{h}} \int_{\mathcal{H}(x,\delta)} \gamma(x,y)(y-x)^{2} b_{i}^{2} dy dx$$

$$-2 \sum_{i=0}^{N} (b_{i+1} - b_{i})^{2} \int_{\Omega_{i}^{h}} \int_{s_{i}}^{x+\delta} \frac{(y-s_{i})(s_{i}-x)}{\delta^{3}} dy dx.$$
(86)

By letting $\gamma(x, y) = \frac{1}{\delta^3} \mathbf{1}_{\{|y-x| < \delta\}}$ and a direct calculation of the above integrals, we get

$$\|w^h\|_{\mathcal{V}}^2 = \frac{2h}{3} \sum_{i=1}^N b_i^2 - \frac{h}{12} \sum_{i=0}^N (b_{i+1} - b_i)^2 = h\left(\frac{2}{3} \sum_{i=1}^N b_i^2 - \frac{1}{12} \sum_{i=1}^{N-1} (b_{i+1} - b_i)^2\right),\tag{87}$$

where the last equality is a result of $b_0 = b_1 = b_N = b_{N+1} = 0$. Therefore,

$$\frac{\sum_{i=0}^{N} |a_{i+1} - a_{i}| |b_{i+1} - b_{i}| O(h)}{\|w^{h}\|_{\mathcal{V}_{0}^{h}}} = \frac{\sum_{i=1}^{N-1} |a_{i+1} - a_{i}| |b_{i+1} - b_{i}| O(h)}{\sqrt{h\left(\frac{2}{3}\sum_{i=1}^{N} b_{i}^{2} - \frac{1}{12}\sum_{i=1}^{N-1} (b_{i+1} - b_{i})^{2}\right)}} \\
\leq O(h) \frac{\sqrt{\sum_{i=1}^{N-1} |a_{i+1} - a_{i}|^{2}} \sqrt{\sum_{i=1}^{N-1} |b_{i+1} - b_{i}|^{2}}}{\sqrt{h\left(\frac{2}{3}\sum_{i=1}^{N} b_{i}^{2} - \frac{1}{12}\sum_{i=1}^{N-1} (b_{i+1} - b_{i})^{2}\right)}} \\
= O(h) \frac{\sqrt{\sum_{i=1}^{N-1} |a_{i+1} - a_{i}|^{2}}}{\sqrt{h\left(\frac{2}{3}(\sum_{i=1}^{N} b_{i}^{2})/(\sum_{i=1}^{N-1} (b_{i+1} - b_{i})^{2}) - \frac{1}{12}\right)}}.$$

Notice that $\sum_{i=1}^{N-1} (b_{i+1} - b_i)^2 = 2 \sum_{i=1}^{N} b_i^2 - 2 \sum_{i=1}^{N-1} b_{i+1} b_i \le 4 \sum_{i=1}^{N} b_i^2$, therefore,

$$\frac{\sum_{i=0}^{N} |a_{i+1} - a_{i}| |b_{i+1} - b_{i}| O(h)}{\|w^{h}\|_{\mathcal{V}}} \leq O(h) \frac{\sqrt{\sum_{i=1}^{N-1} |a_{i+1} - a_{i}|^{2}}}{\sqrt{h\left(\frac{8}{3} - \frac{1}{12}\right)}}$$

$$= O(h) \sqrt{\frac{\sum_{i=1}^{N-1} |a_{i+1} - a_{i}|^{2}}{h}}.$$
(89)

Since v^h is the piecewise linear interpolation of u, then $a_i = u'(x_i)$ for some $x_i \in \Omega_i^h$, so

$$|a_{i+1} - a_i| = |u'(x_{i+1}) - u'(x_i)| = \left| \int_{x_i}^{x_{i+1}} u''(s) ds \right| \le h \int_{x_i}^{x_{i+1}} |u''(s)| ds, \tag{90}$$

where the last inequality comes from Cauchy–Schwartz inequality. Therefore we have $\sqrt{\frac{\sum_{i=1}^{N-1}|a_{i+1}-a_i|^2}{h}} \leq \|u\|_{H^2}$. All together, we have shown

$$\sup_{w^h \in \mathcal{V}_0^h} \frac{|D(v^h, w^h) - D^h(v^h, w^h)|}{\|w^h\|_{\mathcal{V}}} \le Ch\|u\|_{H^2} \tag{91}$$

for $v^h = I_h u$, and therefore the desired result. \square

Remark 5.4. The proof of Theorem 5.3 utilizes the structure of the uniform grid. In particular, (80) and (83) hold only if we have a uniform grid. For quasi-uniform grids, i.e., non-uniform grids with bounded ratio between the maximum mesh size h_{max} and the minimum mesh size h_{min} , we can follow the similar arguments so that (85) is then replaced with

$$\sup_{w^h \in \mathcal{V}_0^h} \frac{\left(\sqrt{\sum_{i=0}^N |a_i|^2} \sqrt{\sum_{i=0}^N |b_i|^2}\right) O(h_{\max})}{\|w^h\|_{\mathcal{V}}}$$

from where one can proceed to show an O(1) estimate of $||u - u^h||_{H^1}$. This estimate will also be numerically verified later.

6. Numerical examples

In this section, we present numerical convergence results obtained by employing the proposed quadrature scheme. We consider one-dimensional and two-dimensional problems discretized on uniform and non-uniform grids.

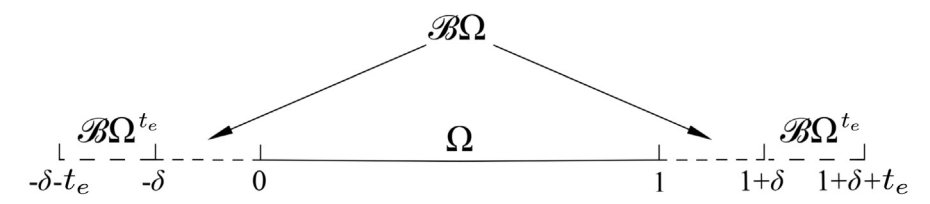


Fig. 9. One-dimensional domain Ω , with associated boundary layer $\mathcal{B}\Omega$. The boundary extension $\mathcal{B}\Omega^{t_e}$ employed in the construction of the inner quadrature points is also represented.

To evaluate the accuracy of the numerical solutions and test the convergence properties of the proposed method, we employ the L^2 and H^1 norms of the difference between the nonlocal numerical solution, u^h , and the analytical solution, u_0 , to a local Poisson problem, i.e.,

$$\|u^{h}(\mathbf{x}) - u_{0}(\mathbf{x})\|_{L^{2}} = \left[\int_{Q} \left(u^{h}(\mathbf{x}) - u_{0}(\mathbf{x})\right)^{2} d\mathbf{x}\right]^{\frac{1}{2}},$$
(92)

and

$$\|u^h(\mathbf{x}) - u_0(\mathbf{x})\|_{H^1} = \left[\int_{\Omega} \left(u^h(\mathbf{x}) - u_0(\mathbf{x}) \right)^2 + \left(\nabla u^h(\mathbf{x}) - \nabla u_0(\mathbf{x}) \right)^2 d\mathbf{x} \right]^{\frac{1}{2}}.$$
 (93)

These norms are computed numerically with Gauss quadrature over the mesh elements, i.e.,

$$\|u^h(\mathbf{x}) - u_0(\mathbf{x})\|_{L^2} \approx \left[\sum_{\Omega_e^h \in \mathcal{M}_{\Omega}^h} \sum_{\mathbf{x}_{gs}^e \in \Omega_e^h} \left(u^h(\mathbf{x}_{gs}) - u_0(\mathbf{x}_{gs}) \right)^2 \omega_{gs} \right]^{\frac{1}{2}}, \tag{94}$$

and

$$\|u^h(\mathbf{x}) - u_0(\mathbf{x})\|_{H^1} \approx \left\{ \sum_{\Omega_e^h \in \mathcal{M}_\Omega^h} \sum_{\mathbf{x}_{gs}^e \in \Omega_e^h} \left[\left(u^h(\mathbf{x}_{gs}) - u_0(\mathbf{x}_{gs}) \right)^2 + \left(\nabla u^h(\mathbf{x}_{gs}) - \nabla u_0(\mathbf{x}_{gs}) \right)^2 \right] \omega_{gs} \right\}^{\frac{1}{2}}, \tag{95}$$

where $\{\mathbf{x}_{gs}\}_{gs=1}^{N_{gs}}$ and $\{\omega_{gs}\}_{gs=1}^{N_{gs}}$, $N_{gs} \in \mathbb{N}$, are the element Gauss quadrature points and weights, respectively. In this work, we take $N_{gs} = 8^d$, where d is the dimension of the problem. Also, in all our numerical examples, we employ fixed ratios $m = \delta/h \in \mathbb{N}$.

6.1. One-dimensional test cases

We consider a one-dimensional domain $\Omega=(0,1)$. For a given horizon δ , its associated interaction domain is $\mathcal{B}\Omega=[-\delta,0]\cup[1,\delta]$ (see Fig. 9). Note that the inner domain, where the function u is unknown (see Eq. (7)), is considered constant in size, while the boundary layer varies with the value of δ . Thus, during our convergence studies, the inner solution domain Ω remains consistent during the refinement ($\delta \to 0$) so that the L^2 error norms associated with each considered value of δ are comparable. We consider the following kernel functions: the constant kernel

$$\gamma_{1,c}(x,y) = \begin{cases} \frac{3}{2\delta^3} & \text{for } |y-x| \le \delta, \\ 0 & \text{for } |y-x| > \delta, \end{cases}$$

$$(96)$$

and the rational kernel

$$\gamma_{1,r}(x,y) = \begin{cases} \frac{1}{\delta^2 |y-x|} & \text{for } |y-x| \le \delta, \\ 0 & \text{for } |y-x| > \delta, \end{cases}$$

$$\tag{97}$$

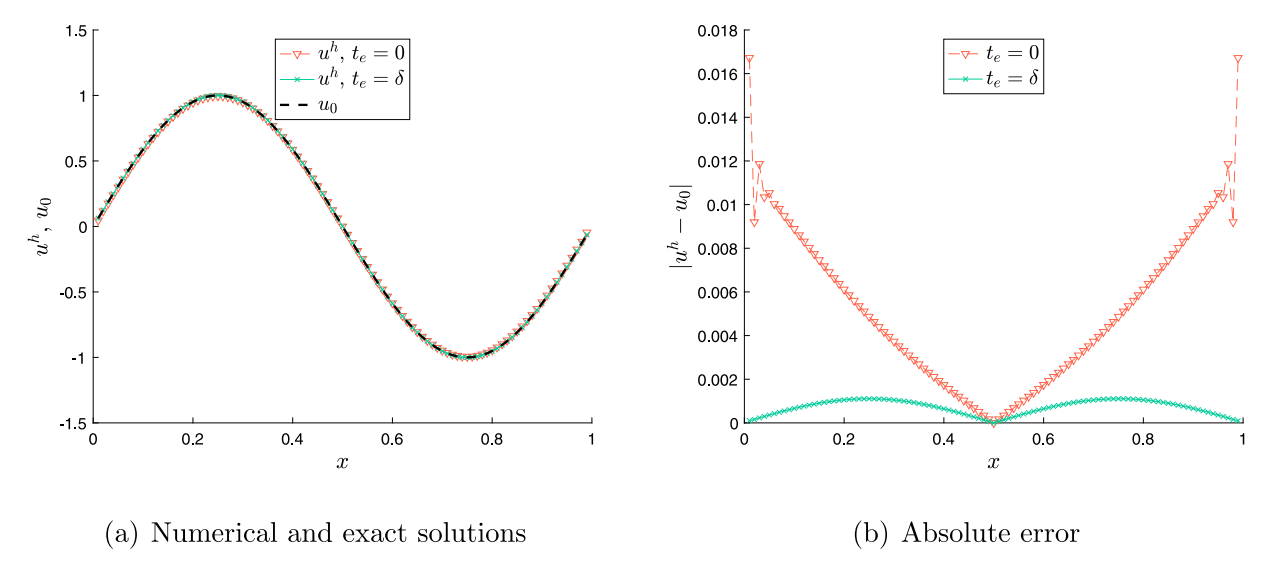


Fig. 10. Numerical solution and associated absolute error for the one-dimensional problem with sinusoidal solution for $\gamma_{1,r}$, m=2, $N_q=40$, and $\overline{N}_{qp}=10$. A uniform element size h=0.01, corresponding to 100 elements for the discretization of Ω is employed.

which correspond to the expressions in Eqs. (4) and (5) for $\zeta_c = 3/2$ and $\zeta_r = 1$, respectively. These values of ζ_c and ζ_r are such that

$$\lim_{\delta \to 0} \mathcal{L}_{\delta} u(x) = \Delta u(x),\tag{98}$$

where Δ is the local Laplace operator. To illustrate the numerical convergence of the proposed method, we consider manufactured solutions, i.e., we choose analytical solutions, $u_0(x)$, to the local Poisson equation and compute the corresponding forcing term b(x) and Dirichlet volume constraint g(x). These are then used for the nonlocal Poisson problem (7). Specifically, we consider two cases: a sinusoidal and a linear solution (with the purpose of performing the so-called patch test). Therefore, for the first case we set $u_0(x) = \sin(2\pi x)$, for which $g(x) = \sin(2\pi x)$ and

$$b(x) = -\Delta u_0(x) = -\Delta \sin(2\pi x) = 4\pi^2 \sin(2\pi x). \tag{99}$$

For the second case, instead, we have $u_0(x) = x$, g(x) = x and

$$b(x) = 0. ag{100}$$

6.1.1. Uniform discretizations

We investigate the convergence behavior for uniform discretizations. The finite element mesh has a uniform discretization size, h, over $[-\delta, 1 + \delta] = ([-\delta, 0] \cup [1, \delta]) \cup (0, 1)$. Recall that we consider cases for which $m = \delta/h \in \mathbb{N}$, meaning that elements of size h subdivide (0, 1) and $[-\delta, 1 + \delta]$ exactly. The same applies when the domain extension $[-\delta - t_e, 1 + \delta + t_e]$, with $t_e = \delta$, is employed. For the outer quadrature, we consider $N_q = 40$ Gauss points, while for inner quadrature we use $\overline{N}_{qp} = 10$.

For the sinusoidal solution we use $\gamma_{1,r}$, h=0.01, and m=2, meaning that Ω is discretized using 100 elements and $\delta=0.02$. For the construction of the inner quadrature weights, we consider two cases: one without domain extension, i.e., $t_e=0$, and one with domain extension $t_e=\delta$. The obtained numerical solutions are reported in Fig. 10(a), while Fig. 10(b) shows the absolute error obtained for the two considered cases. We observe that, when $t_e=0$, the error concentrates near the boundary of the domain, whereas this does not occur for $t_e=\delta$. Next, we perform an L^2 norm convergence study by varying h and δ , with fixed ratio m=2. As shown in Fig. 11, for $t_e=0$, we observe a linear convergence, whereas, for $t_e=\delta$, the rate is quadratic. This suggests that the concentration of error near the boundary observed for $t_e=0$ reduces the overall convergence rate. Therefore, from now on, we only employ $t_e=\delta$ in the construction of the inner quadrature weights.

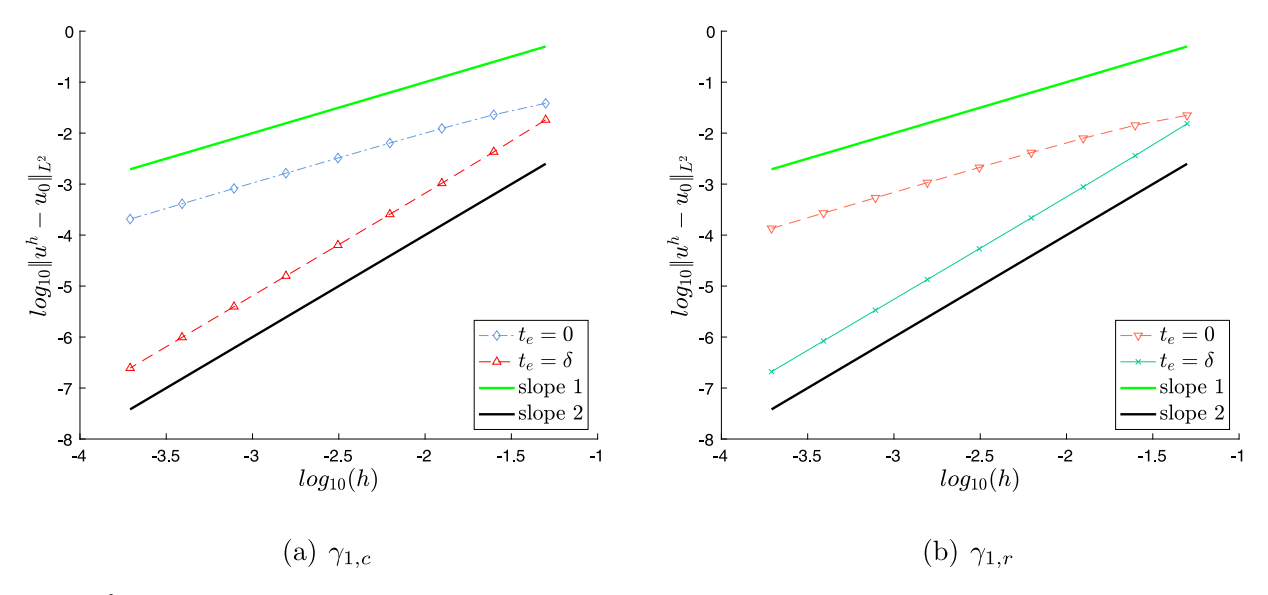


Fig. 11. L^2 norm convergence behaviors of the one-dimensional numerical solutions for the case with sinusoidal solution. m=2, uniform discretization, and $t_e=0$ and $t_e=\delta$. $N_q=40$ and $\overline{N}_{qp}=10$ are employed. $\gamma_{1,c}$ and $\gamma_{1,r}$ are both considered.

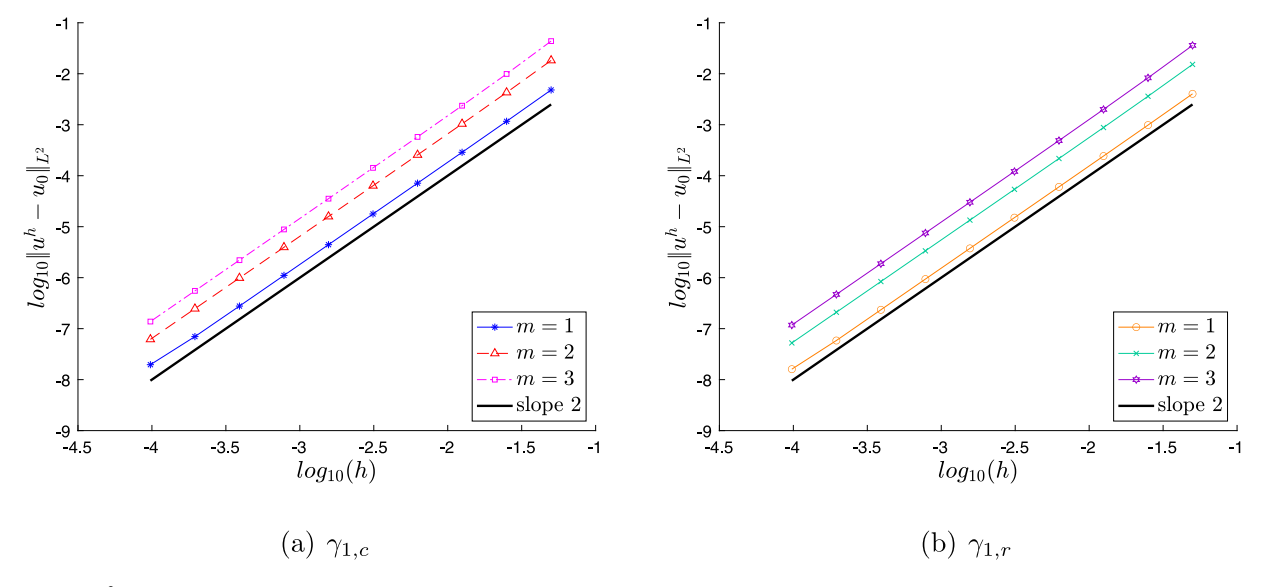


Fig. 12. L^2 norm convergence behaviors of the one-dimensional numerical solutions for the case with sinusoidal solution. m=1,2,3, uniform discretization, and $t_e=\delta$. $N_q=40$ and $\overline{N}_{qp}=10$ are employed. $\gamma_{1,c}$ and $\gamma_{1,r}$ are both considered.

Figs. 12(a) and 12(b) show the L^2 norm convergence behavior for $\gamma_{1,c}$ and $\gamma_{1,r}$, respectively. For both cases, we employ $t_e = \delta$. $N_q = 40$, and $\overline{N}_{qp} = 10$. For all considered values of m (i.e., m = 1, 2, 3), we observe a second-order convergence rate in the L^2 norm. The convergence behavior in the H^1 norm is presented in Fig. 13. For all of the considered cases, a first-order convergence is obtained, which is consistent with the theoretical prediction from Section 5. It can also be noted that convergence in the H^1 norm is one rate lower than in L^2 .

To further investigate the performance of the optimization-based approach, in B, we compare its results for this problem with those obtained by employing Gauss quadrature over the element-ball intersections for the inner integral operator.

Next, we consider the case with a linear solution. For the reasons illustrated above, we consider $t_e = \delta$; we set h = 0.01 and m = 2, meaning that Ω is discretized using 100 elements and $\delta = 0.02$. The L^2 norms of the error for

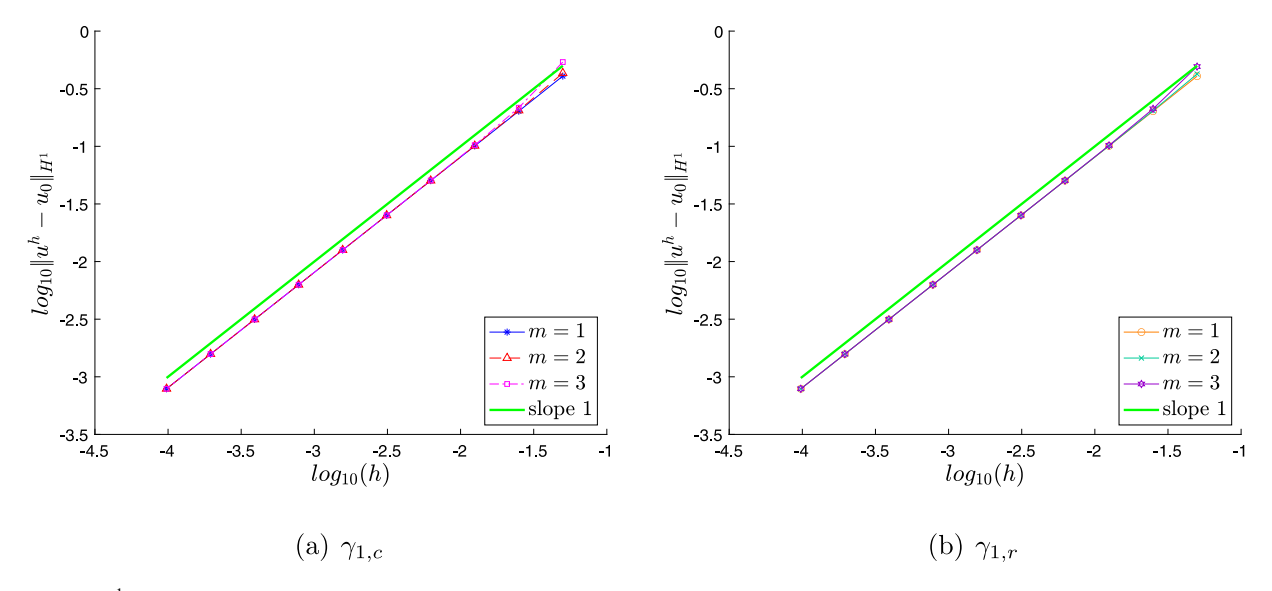


Fig. 13. H^1 norm convergence behaviors of the one-dimensional numerical solutions for the case with sinusoidal solution. m=1,2,3, uniform discretization, and $t_e=\delta$. $N_q=40$ and $\overline{N}_{qp}=10$ are employed. $\gamma_{1,c}$ and $\gamma_{1,r}$ are both considered.

the cases with $\gamma_{1,r}$ and $\gamma_{1,c}$ are 1.59E-13 and 6.96E-14, respectively. This fact implies that the proposed approach passes the patch test for uniform discretizations, i.e., the numerical solution is accurate up to machine precision for linear solutions. This is expected since the exact, local solution belongs to the discretization space \mathcal{V}^h .

6.1.2. Nonuniform discretizations

Next, we investigate the performance of the proposed method for non-uniform discretizations. The non-uniform discretizations are constructed by perturbing uniform discretizations of size h. This is achieved by moving each finite element node in (0, 1) and $(-\delta, 0) \cup (1, 1 + \delta)$ from their original position x^u to a new randomly selected position $x^{nu} = x^u + \epsilon h R_a$, where ϵ is a chosen perturbation factor and R_a is a random number in [-1, 1].

As for uniform discretizations, we first consider the sinusoidal solution. We select $t_e = \delta$, $N_q = 40$, and $\overline{N}_{qp} = 10$. Figs. 14 and 15 show the convergence behavior for m = 2,3 for both $\gamma_{1,c}$ and $\gamma_{1,r}$, in the L^2 and H^1 norms, respectively. We observe an apparent second-order convergence rate in the L^2 , and first-order for the H^1 norm, i.e., one rate lower. However, it should be noted that Fig. 15 shows a reduction in the H^1 convergence rate for the finer cases, suggesting that, asymptotically, the convergence rate may reach a zeroth-order convergence, as discussed in Remark 5.4.

We then consider the linear solution. As before, we take $t_e = \delta$, $N_q = 40$, and $\overline{N}_{qp} = 10$. In contrast to the uniform case, for non-uniform discretizations, the proposed method does not pass the patch test. As shown in Figs. 16 and 17, which report convergence behavior in the L^2 and H^1 norms, respectively, for m = 2, 3 for $\gamma_{1,c}$ and $\gamma_{1,r}$, the method shows a first-order L^2 norm convergence and a zeroth-order H^1 norm convergence (see Remark 5.4). By comparing Figs. 14 and 16, it can be noted that the magnitude of the L^2 norm errors obtained for the case with a linear solution is much smaller compared with the magnitude obtained for the problem with a sinusoidal solution. This confirms our conjecture that the method has a first-order asymptotic convergence in the L^2 norm, and that second-order convergence is observed in the pre-asymptotic regime.

A natural question is whether further refinement of the sinusoidal case would show a reduction in convergence rate in the L^2 norm; we note that attempting to refine the sinusoidal case further, the error becomes dominated by floating point arithmetic. Nonetheless, since, as shown in Fig. 15, the convergence rate in the H^1 norm starts to reduce for the finer refinements, and we have observed one-order lower convergence in the L^2 norm, it is reasonable to expect that the convergence rate in the L^2 norm would reduce with further refinement.

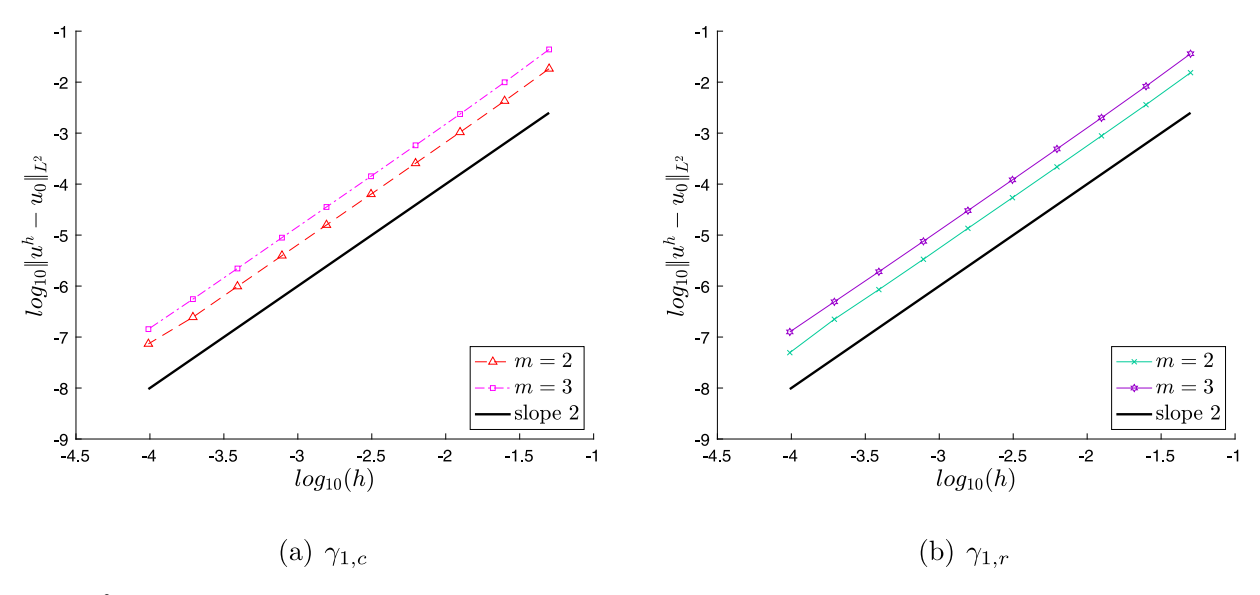


Fig. 14. L^2 convergence behaviors of the one-dimensional numerical solutions for the case with sinusoidal solution. m=2,3, non-uniform discretization with $\epsilon=0.1$, and $t_e=\delta$. $N_q=40$ and $\overline{N}_{qp}=10$ are employed. $\gamma_{1,c}$ and $\gamma_{1,r}$ are both considered.

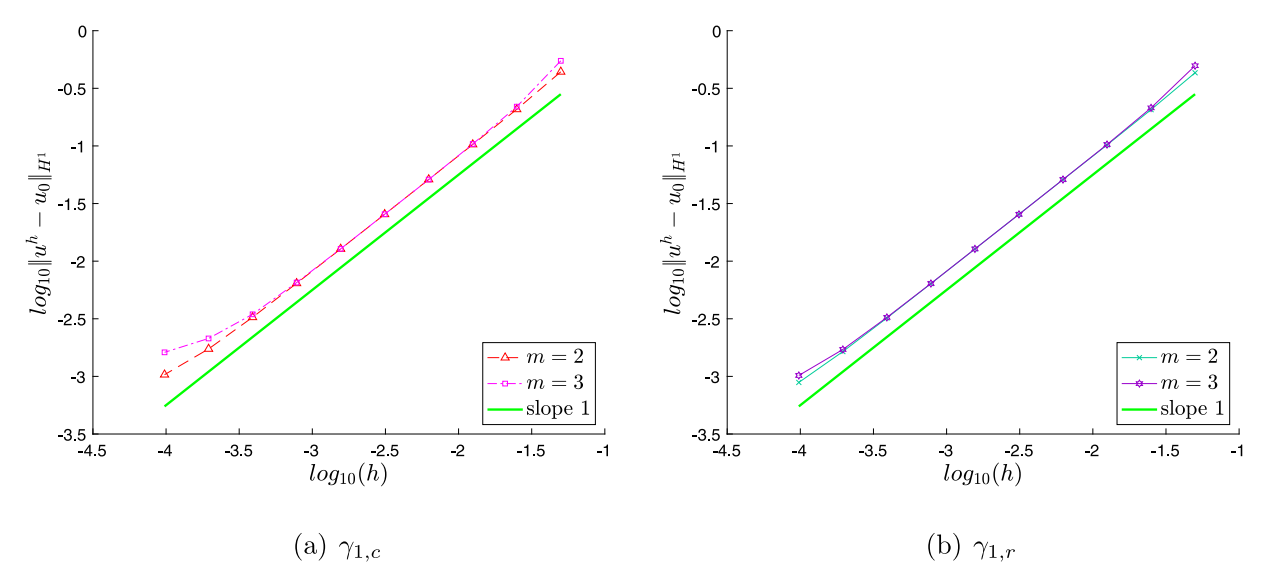


Fig. 15. H^1 norm convergence behaviors of the one-dimensional numerical solutions for the case with sinusoidal solution. m=2,3, non-uniform discretization with $\epsilon=0.1$, and $t_e=\delta$. $N_q=40$ and $\overline{N}_{qp}=10$ are employed. $\gamma_{1,c}$ and $\gamma_{1,r}$ are both considered.

6.2. Two-dimensional test cases

We consider the two-dimensional domain $\Omega=(0,1)\times(0,1)$ with associated interaction domain $\mathcal{B}\Omega=([-\delta,1+\delta]\times[-\delta,1+\delta])\setminus\Omega$ (see Fig. 18). As in the previous section, this guarantees that in the convergence studies the inner solution domain Ω remains consistent during the refinement $(\delta\to 0)$, so that the L^2 error norms are comparable for all δ . We consider two kernel functions: a constant influence function

$$\gamma_{2,c}(\mathbf{x}, \mathbf{y}) = \begin{cases} \frac{4}{\pi \delta^4} & \text{for } |\mathbf{y} - \mathbf{x}|_{\ell^2} \le \delta, \\ 0 & \text{for } |\mathbf{y} - \mathbf{x}|_{\ell^2} > \delta, \end{cases}$$
(101)

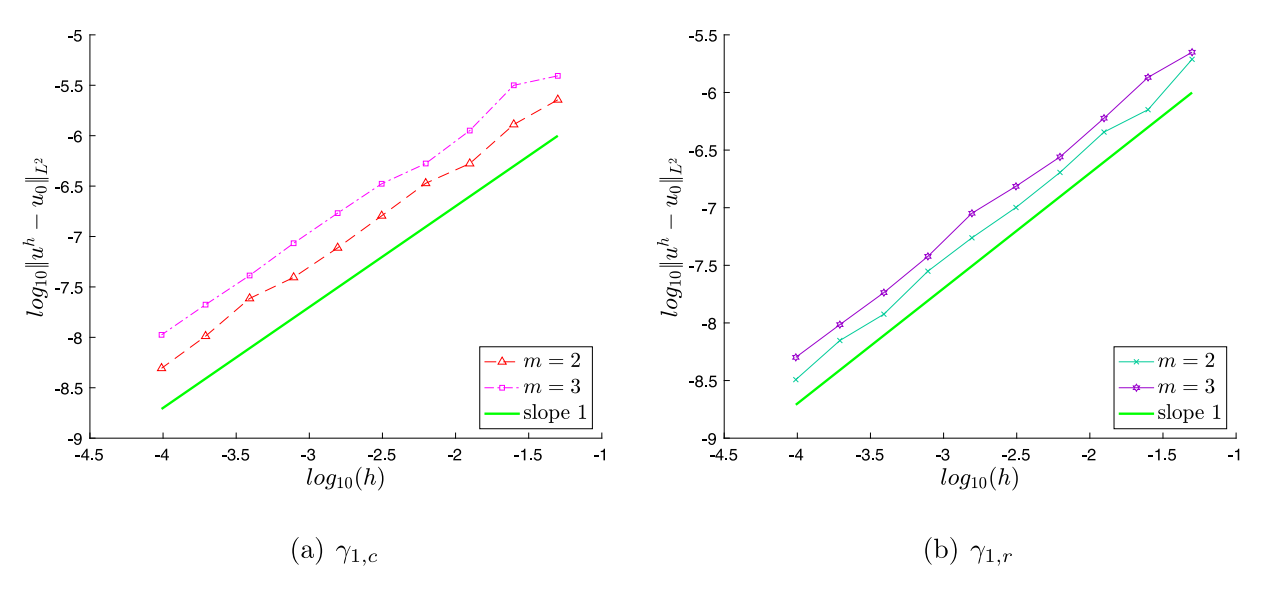


Fig. 16. L^2 norm convergence behaviors of the one-dimensional numerical solutions for the case with linear solution. m=2,3, non-uniform discretization with $\epsilon=0.1$, and $t_e=\delta$. $N_q=40$ and $\overline{N}_{qp}=10$ are employed. $\gamma_{1,c}$ and $\gamma_{1,r}$ are both considered.

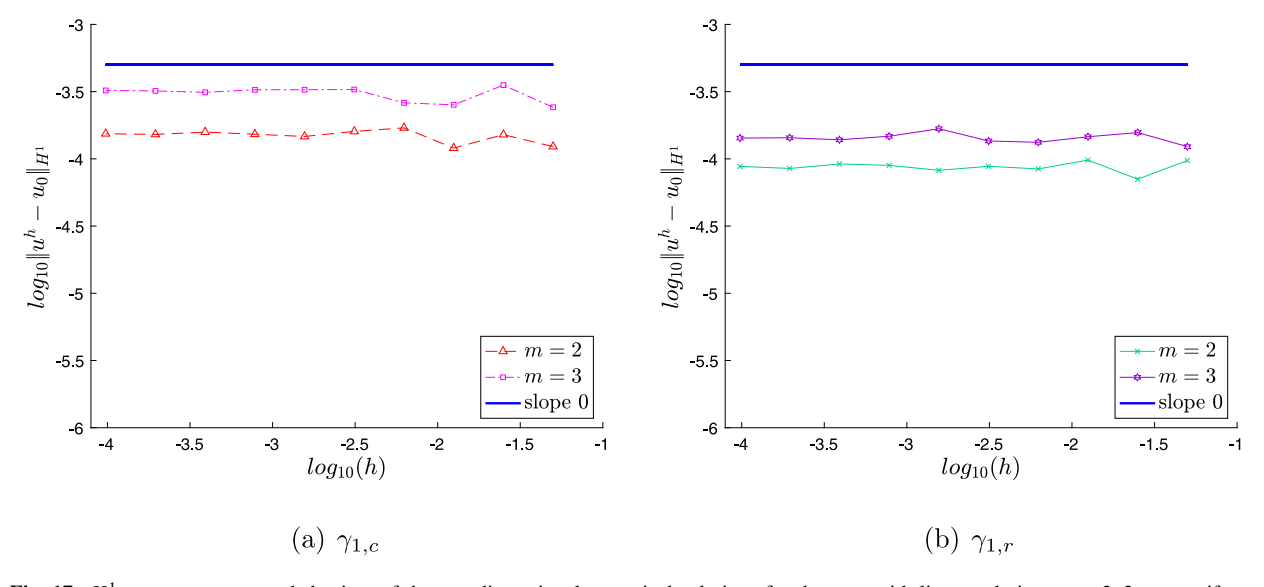


Fig. 17. H^1 norm convergence behaviors of the one-dimensional numerical solutions for the case with linear solution. m=2,3, non-uniform discretization with $\epsilon=0.1$, and $t_e=\delta$. $N_q=40$ and $\overline{N}_{qp}=10$ are employed. $\gamma_{1,c}$ and $\gamma_{1,r}$ are both considered.

and a rational one

$$\gamma_{2,r}(\mathbf{x}, \mathbf{y}) = \begin{cases} \frac{3}{\pi \delta^3 |\mathbf{y} - \mathbf{x}|_{\ell^2}} & \text{for } |\mathbf{y} - \mathbf{x}|_{\ell^2} \le \delta, \\ 0 & \text{for } |\mathbf{y} - \mathbf{x}|_{\ell^2} > \delta, \end{cases}$$
(102)

which correspond to the expressions in Eqs. (4) and (5) for $\zeta_c = 4/\pi$ and $\zeta_r = 3/\pi$, respectively. As for the one-dimensional case, these values of ζ_c and ζ_r are such that

$$\lim_{\delta \to 0} \mathcal{L}_{\delta} u(\mathbf{x}) = \Delta u(\mathbf{x}). \tag{103}$$

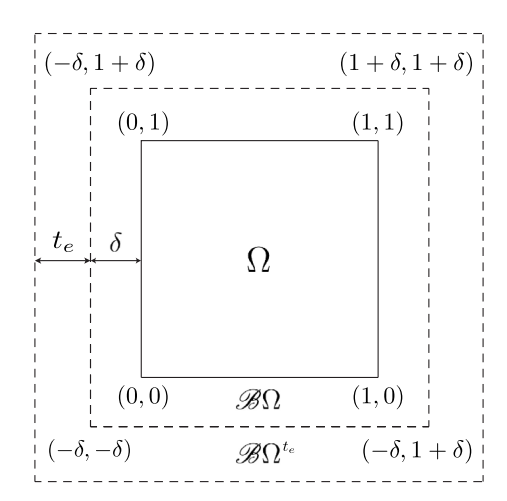


Fig. 18. Two-dimensional domain Ω , with associated boundary layer $\mathcal{B}\Omega$. The boundary extension $\mathcal{B}\Omega^{l_e}$ employed in the construction of the inner quadrature points is also represented.

As discussed in Section 2, the supports of the kernels presented in (101) and (102) correspond to circular Euclidean ℓ^2 balls. However, kernels associated with ℓ^∞ balls (i.e., square supports) were also investigated and similar results as the ones presented in this section for Euclidean balls were obtained. As before, we employ the method of manufactured solutions. We select $u_0(\mathbf{x}) = \sin(2\pi x_1)\sin(2\pi x_2)$, where $\mathbf{x} = (x_1, x_2)$, which corresponds to $g(\mathbf{x}) = \sin(2\pi x_1)\sin(2\pi x_2)$ and to the following source term:

$$b(\mathbf{x}) = -\Delta u_0(\mathbf{x}) = -\Delta \left(\sin(2\pi x_1)\sin(2\pi x_2)\right) = 8\pi^2 \sin(2\pi x_1)\sin(2\pi x_2). \tag{104}$$

6.2.1. Uniform discretizations

As for the one-dimensional case, we first investigate the convergence behavior for uniform discretizations. The two-dimensional uniform mesh is constructed as a tensor product $\mathcal{M}_2^{h,u} = \mathcal{M}_{x_2}^{h,u} \times \mathcal{M}_{x_1}^{h,u}$, where $\mathcal{M}_{x_1}^{h,u}$ and $\mathcal{M}_{x_2}^{h,u}$ are one-dimensional uniform meshes of size h over $[-\delta,0] \cup (0,1) \cup [1,1+\delta]$. For the convergence study, we set $t_e = \delta$, $\overline{N}_{qp} = 64$, and use a four by four Gauss quadrature rule for the outer integral $(N_q = 16)$. Figs. 19(a) and 19(b) show the obtained results for $\gamma_{2,c}$ and $\gamma_{2,r}$, respectively. Up to the considered level of refinement, we observe a second-order convergence rate in the L^2 norm for both kernels.

6.2.2. Nonuniform discretizations

In this section, we investigate the performance of the proposed quadrature approach for two-dimensional non-uniform discretizations. We construct the two-dimensional non-uniform mesh as a tensor product of one-dimensional non-uniform discretization, i.e., $\mathcal{M}_2^{h,nu} = \mathcal{M}_{x_1}^{h,nu} \times \mathcal{M}_{x_2}^{h,nu}$, where $\mathcal{M}_{x_1}^{h,nu}$ and $\mathcal{M}_{x_2}^{h,nu}$ are obtained by perturbing $\mathcal{M}_{x_1}^{h,u}$ and $\mathcal{M}_{x_2}^{h,u}$, which are uniform meshes with spacing h over $[-\delta,0] \cup (0,1) \cup [1,1+\delta]$. Similarly to the one-dimensional non-uniform case, the perturbation is achieved by moving the finite element nodes in (0,1) and $(-\delta,0) \cup (1,1+\delta)$ from their original positions x_1^u and x_2^u to new randomly selected positions $x_1^{nu} = x_1^u + \epsilon h R_a$ and $x_2^{nu} = x_2^u + \epsilon h R_a$, where ϵ is a chosen perturbation factor and R_a is a random number in [-1,1]. For a visual example of $\mathcal{M}_2^{h,nu}$, see Fig. 20.

For the convergence studies we use $t_e = \delta$, $\overline{N}_{qp} = 64$, and $N_q = 16$ (four by four Gauss quadrature), with $\epsilon = 0.1$. Figs. 21(a) and 21(b) show the results for $\gamma_{2,c}$ and $\gamma_{2,r}$, respectively. Up to the considered level of refinement, we observe a second-order convergence rate in the L^2 norm for both kernels also for the non-uniform case. As discussed in more detail for the one-dimensional nonuniform case in Section 6.1.2, we conjecture that this rate is pre-asymptotic, and that the first-order asymptotic regime is difficult to observe in practice.

7. Conclusions

We proposed a novel quadrature rule for the computation of integrals that arise in the matrix assembly of finite-element discretizations of nonlocal problems. In contrast to all previously employed methods, our technique

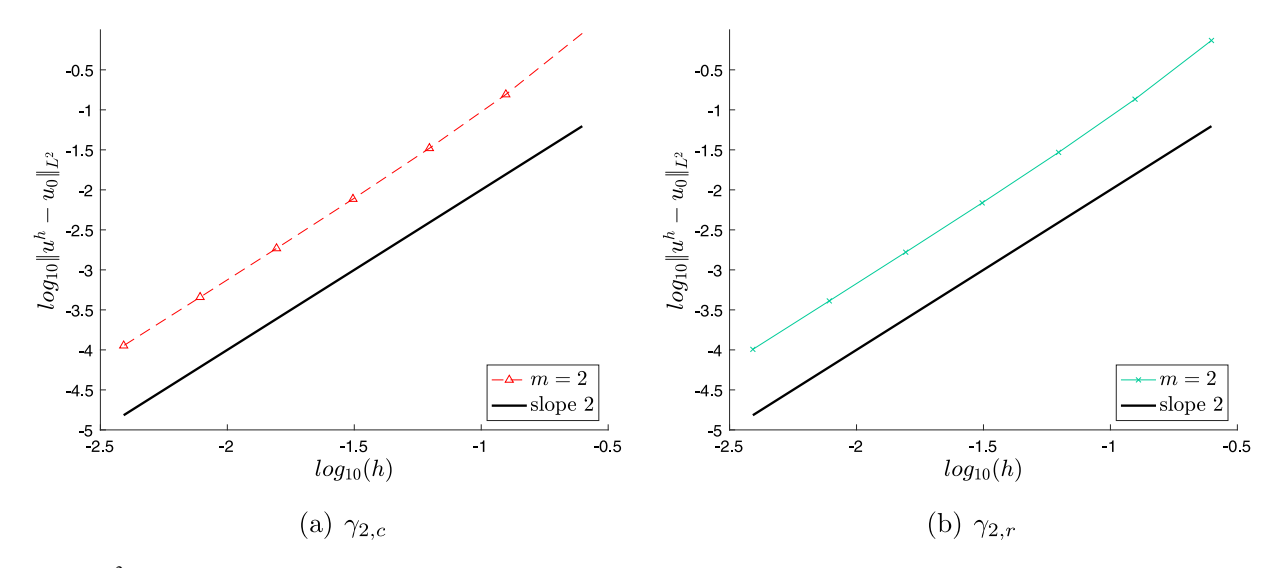


Fig. 19. L^2 convergence behaviors of the two-dimensional numerical solutions for m=2, uniform discretization, and $t_e=\delta$. $N_q=16$ (as 4×4) and $\overline{N}_{qp}=64$. $\gamma_{2,c}$ and $\gamma_{2,r}$ are both considered.

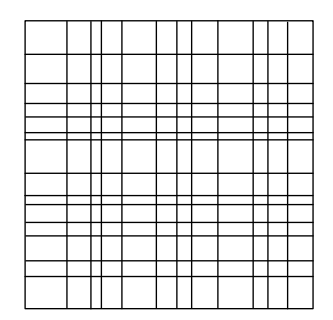


Fig. 20. Example of two-dimensional non-uniform mesh obtained as a tensor product of perturbed one-dimensional meshes.

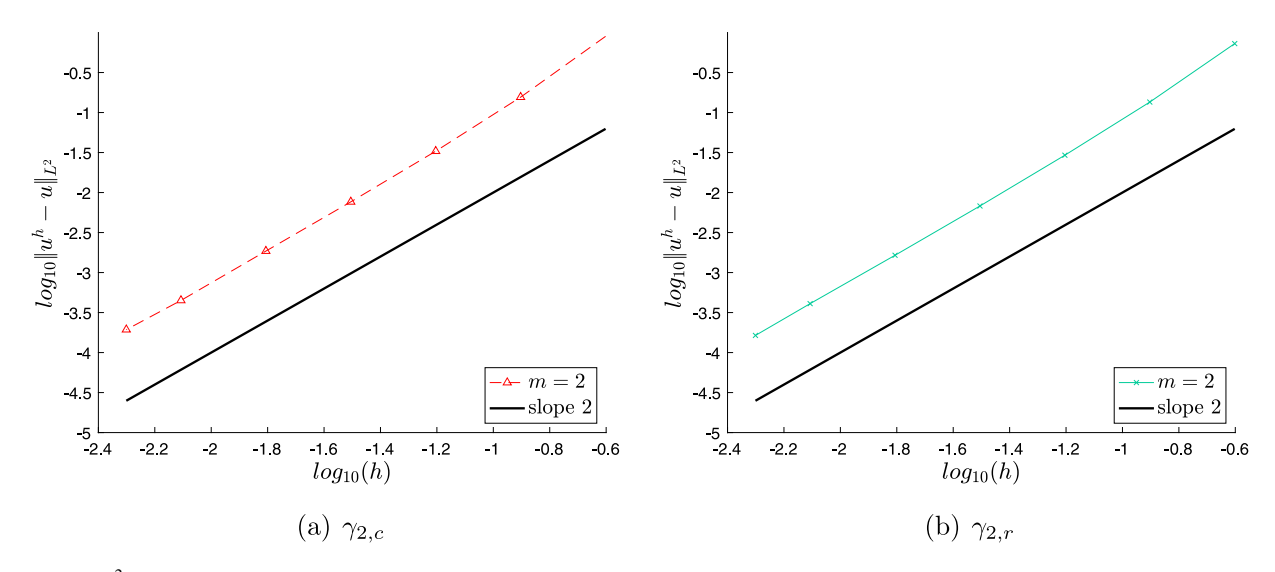


Fig. 21. L^2 convergence behaviors of the two-dimensional numerical solutions for m=2, non-uniform discretization with $\epsilon=0.1$, and $t_e=\delta$. $N_q=16$ (as 4 \times 4) and $\overline{N}_{qp}=64$. $\gamma_{2,c}$ and $\gamma_{2,r}$ are both considered.

does not require element-by-element integration, but relies on global integration over the nonlocal neighborhood. Specifically, we consider quadrature rules based on the generalized moving least squares method where the (global) quadrature weights are obtained by solving an equality-constrained optimization problem. The major advantage of this technique is the fact that the computation of element-ball intersections, a nontrivial and time consuming task, is avoided. Additionally, this technique requires minimal implementation effort, as it can be implemented in an existing finite element code. For this reason, we expect the proposed approach to become a building block of agile engineering codes. Our numerical experiments show that, when boundary conditions are treated carefully and the outer integral is computed accurately, our method is asymptotically compatible in the limit of $h \sim \delta \to 0$, featuring at least first-order convergence in L^2 for all dimensions and for both uniform and nonuniform grids. For piecewise linear finite-element implementations, in the case of uniform grids, our method features an optimal, second-order convergence rate in L^2 and passes the patch test. For nonuniform grids, we see effective second-order convergence over a long pre-asymptotic regime, whereas the asymptotic first-order convergence is only evident in deviations from the patch test, which are very small relative to errors in more complicated solutions. Convergence rates in H^1 are consistently one order lower than the L^2 rates.

We also carry out a preliminary numerical analysis of the method, but using the H^1 norm and restricted to the case of $h = \delta$ in one spatial dimension. This analysis is consistent with the convergence rates observed in numerical experiments, but it does not account for the increase in convergence rate when measuring the L^2 norm instead of H^1 . As such, we believe that an interesting future direction for numerical analysis of this quadrature scheme would be to obtain sharp L^2 error estimates.

Declaration of competing interest

The authors declare that they have no known competing financial interests or personal relationships that could have appeared to influence the work reported in this paper.

Acknowledgments

Kamensky and Pasetto were supported by start-up funding from the University of California San Diego, USA. The work of Tian was partially supported by the National Science Foundation, USA grant DMS-2111608. D'Elia and Trask are supported by the Sandia National Laboratories (SNL), USA Laboratory-directed Research and Development program and by the U.S. Department of Energy, Office of Advanced Scientific Computing Research under the Collaboratory on Mathematics and Physics-Informed Learning Machines for Multiscale and Multiphysics Problems (PhILMs) project. SNL is a multimission laboratory managed and operated by National Technology and Engineering Solutions of Sandia, LLC., a wholly owned subsidiary of Honeywell International, Inc., for the U.S. Department of Energy's National Nuclear Security Administration under contract DE-NA0003525. This paper, SAND2022-0834, describes objective technical results and analysis. Any subjective views or opinions that might be expressed in this paper do not necessarily represent the views of the U.S. Department of Energy or the United States Government.

Appendix A. One-dimensional inner quadrature weights

In this appendix, in order to verify the assumptions on the optimization-based quadrature weights employed in Section 5.2.1, we derive explicit expressions for the optimization-based inner quadrature weights in a one-dimensional setting and for the constant kernel function $\gamma(x,y) = \frac{\zeta}{\delta^3}$ defined in (4). Recall from Section 4.2 that the inner quadrature points are positioned in $\mathcal{H}(x,\delta)$ according to

$$x_{qp} = x_q + (2k - \operatorname{sgn}(k))\frac{\overline{h}}{2}, \quad -\overline{N}_{qp,\delta} \le k \le \overline{N}_{qp,\delta}$$
(A.1)

with $k \in \mathbb{Z} \setminus \{0\}$ and

$$\overline{h} = \frac{\delta}{\overline{N}_{qp,\delta}} = \frac{m}{\overline{N}_{qp,\delta}} h = \upsilon h, \tag{A.2}$$

where we defined $v = m/\overline{N}_{qp,\delta}$. We then start by considering the constant kernel in Eq. (4). Following the procedure outlined in Section 3, we have

$$\mathbf{B} = \frac{\zeta_c}{\delta^3} \left[\left(x_q - x_{-\overline{N}_{qp,\delta}} \right)^2 \dots \left(x_q - x_i \right)^2 \dots \left(x_q - x_{\overline{N}_{qp,\delta}} \right)^2 \right]$$

$$= \frac{\zeta_c \overline{h}^2}{4\delta^3} \left[\left(-2N_{qp,\delta} - \operatorname{sgn}(-N_{qp,\delta}) \right)^2 \dots \left(2i - \operatorname{sgn}(i) \right)^2 \dots \left(2N_{qp,\delta} - \operatorname{sgn}(N_{qp,\delta}) \right)^2 \right]$$
(A.3)

and

$$S = \mathbf{B}\mathbf{B}^{T} = \frac{\zeta_{c}^{2}\overline{h}^{4}}{16\delta^{6}} \sum_{\substack{k=-\overline{N}_{qp,\delta} \\ k \neq 0}}^{\overline{N}_{qp,\delta}} \left[2(k) - \operatorname{sgn}(k) \right]^{4} = \frac{\zeta_{c}^{2}\overline{h}^{4}}{16\delta^{6}} \left[\frac{2}{15} \left(7\overline{N}_{qp,\delta} - 40\overline{N}_{qp,\delta}^{3} + 48\overline{N}_{qp,\delta}^{5} \right) \right], \tag{A.4}$$

which leads to

$$S^{-1} = \frac{16\delta^6}{\zeta_c^2 \overline{h}^4} \frac{1}{\left[\frac{2}{15} \left(7\overline{N}_{qp,\delta} - 40\overline{N}_{qp,\delta}^3 + 48\overline{N}_{qp,\delta}^5\right)\right]}.$$
 (A.5)

For the choice of V_h defined in (48),

$$g = \frac{2}{3}\zeta_c. \tag{A.6}$$

Therefore, from Eqs. (27), (A.1), (A.3), (A.5), and (A.6)

$$\frac{1}{2} = \frac{\zeta_{c}\overline{h}^{2}}{4\delta^{3}} \begin{bmatrix} (-2\overline{N}_{qp,\delta} - \operatorname{sgn}(-\overline{N}_{qp,\delta}))^{2} \\ (2i - \operatorname{sgn}(i))^{2} \\ \dots \\ (2\overline{N}_{qp,\delta} - \operatorname{sgn}(\overline{N}_{qp,\delta}))^{2} \end{bmatrix} \frac{16\delta^{6}}{\zeta_{c}^{2}\overline{h}^{4}} \frac{1}{\left[\frac{2}{15}\left(7\overline{N}_{qp,\delta} - 40\overline{N}_{qp,\delta}^{3} + 48\overline{N}_{qp,\delta}^{5}\right)\right]} \frac{2}{3}\zeta_{c}$$

$$= \frac{8\delta^{3}}{3\overline{h}^{2}} \frac{1}{\left[\frac{2}{15}\left(7\overline{N}_{qp,\delta} - 40\overline{N}_{qp,\delta}^{3} + 48\overline{N}_{qp,\delta}^{5}\right)\right]} \begin{bmatrix} (-2\overline{N}_{qp,\delta} - \operatorname{sgn}(-\overline{N}_{qp,\delta}))^{2} \\ \dots \\ (2i - \operatorname{sgn}(i))^{2} \\ \dots \\ (2\overline{N}_{qp,\delta} - \operatorname{sgn}(\overline{N}_{qp,\delta}))^{2} \end{bmatrix}$$

$$= \frac{8\delta\left(\overline{N}_{qp,\delta}\right)^{2}}{3\left[\frac{2}{15}\left(7\overline{N}_{qp,\delta} - 40\overline{N}_{qp,\delta}^{3} + 48\overline{N}_{qp,\delta}^{5}\right)\right]} \begin{bmatrix} (-2\overline{N}_{qp,\delta} - \operatorname{sgn}(-\overline{N}_{qp,\delta}))^{2} \\ \dots \\ (2\overline{N}_{qp,\delta} - \operatorname{sgn}(\overline{N}_{qp,\delta}))^{2} \end{bmatrix}$$

$$= \frac{8\delta\overline{N}_{qp,\delta}}{3\left[\frac{2}{15}\left(7 - 40\overline{N}_{qp,\delta}^{2} + 48\overline{N}_{qp,\delta}^{4}\right)\right]} \begin{bmatrix} (-2\overline{N}_{qp,\delta} - \operatorname{sgn}(-\overline{N}_{qp,\delta}))^{2} \\ \dots \\ (2i - \operatorname{sgn}(i))^{2} \\ \dots \\ (2i - \operatorname{sgn}(i)^{2} \\ \dots \\$$

It has to be noted that, for $\overline{N}_{qp,\delta} \in \mathbb{N}$, $\omega_k > 0$, $\forall k$. Therefore, in this case, all the quadrature weights are positive and there exists a generic constant C > 0 independent of h and δ , such that $C\delta < \omega_{\min}$, with $\omega_{\min} = \min_k \{\omega_k\}$.

Similarly, for kernels of the type in Eq. (5), we get

$$\mathbf{B} = \frac{\zeta_r}{\delta^2} \left[\frac{\left(x_q - x_{-\overline{N}_{qp,\delta}} \right)^2}{\left| x_q - x_{-\overline{N}_{qp,\delta}} \right|^2} \dots \frac{\left(x_q - x_i \right)^2}{\left| x_q - x_i \right|} \dots \frac{\left(x_q - x_{\overline{N}_{qp,\delta}} \right)^2}{\left| x_q - x_{\overline{N}_{qp,\delta}} \right|} \right]$$

$$= \frac{\zeta_r \overline{h}}{2\delta^2} \left[\left| -2N_{qp,\delta} - \operatorname{sgn}(-N_{qp,\delta}) \right| \dots \left| 2i - \operatorname{sgn}(i) \right| \dots \left| 2N_{qp,\delta} - \operatorname{sgn}(N_{qp,\delta}) \right| \right]$$
(A.8)

and

$$S = \mathbf{B}\mathbf{B}^{T} = \frac{\zeta_{r}^{2}\overline{h}^{2}}{4\delta^{4}} \sum_{\substack{k = -\overline{N}_{qp,\delta} \\ k \neq 0}}^{\overline{N}_{qp,\delta}} \left[2(k) - \operatorname{sgn}(k) \right]^{2} = \frac{\zeta_{r}^{2}\overline{h}^{2}}{4\delta^{4}} \left[\frac{2}{3} \left(-\overline{N}_{qp,\delta} + 4\overline{N}_{qp,\delta}^{3} \right) \right], \tag{A.9}$$

which leads to

$$S^{-1} = \frac{4\delta^4}{\zeta_r^2 \overline{h}^2} \frac{1}{\left[\frac{2}{3} \left(-\overline{N}_{qp,\delta} + 4\overline{N}_{qp,\delta}^3\right)\right]}.$$
(A.10)

For the choice of V_h defined in (48),

$$g = \zeta_r. \tag{A.11}$$

Therefore, from Eqs. (27), (A.1), (A.8), (A.10), and (A.11)

As before, for $\overline{N}_{qp,\delta} \in \mathbb{N}$, $\omega_k > 0$, $\forall k$. Therefore, in this case, all the quadrature weights are positive and there exists a generic constant C > 0 independent of h and δ , such that $C\delta < \omega_{\min}$, with $\omega_{\min} = \min_k \{\omega_k\}$.

Appendix B. One-dimensional comparison with Gauss quadrature over element-ball intersections

In this appendix, we consider the one-dimensional problem with exact local sinusoidal solution and uniform discretization introduced in Section 6.1.1 and compare the solutions obtained by using, for the inner integral operator, the optimization-based quadrature approach (see Sections 3 and 4) with the solutions obtained by using Gauss quadrature over the element-ball intersections. For the outer integral, Gauss quadrature is employed in both

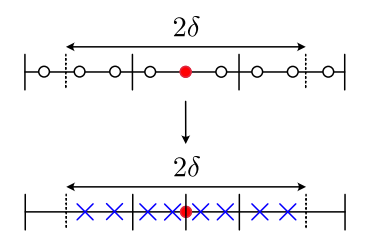


Fig. B.22. One-dimensional Gauss quadrature approach for both outer and inner integrals. The filled red dot represents x_q^e while the blue crosses are the associated Gauss quadrature points x_q^c over each Ω_i^c .

approaches. Therefore, as in Section 4.2, we start by numerically integrating the outer integral over the finite element mesh \mathcal{M}^h in $D(u^h, v^h)$ by using $N_q \in \mathbb{N}$ Gauss points $\left\{x_q^e\right\}_{q=1}^{N_q}$ (with associated weights $\left\{\omega_q^e\right\}_{q=1}^{N_q}$) over each element Ω_a^h :

$$D(u^h, v^h) \approx \sum_{\Omega_e^h \in \mathcal{M}^h} \sum_{q=1}^{N_q} \int_{(\Omega \cup \mathcal{B}\Omega) \cap \mathcal{H}(x_q^e, \delta)} \left[v^h(y) - v^h(x_q^e) \right] \gamma(x_q^e, y) \left[u^h(y) - u^h(x_q^e) \right] dy \omega_q^e, \tag{B.1}$$

Let us now describe the approach employed for approximating remaining integral in Eq. (B.1) by numerically integrating over the element–ball intersections. Recalling that $\{\tilde{x}_j\}_{j=1}^J$, with $J \in \mathbb{N}$, is the set of all the nodes in \mathcal{M}^h , we define a set

$$\left\{x_{qk}^{e}\right\}_{k=1}^{N_K} := \left(\left\{\tilde{x}_{j}\right\}_{j=1}^{J} \cup \left\{x_{q}^{e} - \delta, x_{q}^{e}, x_{q}^{e} + \delta\right\}\right) \cap \mathcal{H}(x_{q}^{e}, \delta) \cap (\Omega \cup \mathcal{B}\Omega), \tag{B.2}$$

with $N_K \in \mathbb{N}$. The set $\left\{x_{qk}^e\right\}_{k=1}^{N_K}$ is ordered, i.e., $x_{q1}^e < x_{q2}^e < \cdots < x_{qN_K}^e$. We now define a set of segments

$$\mathcal{M}^{\cap} := \{\Omega_i^{\cap}\}_{i=1,\dots,N_K-1} \tag{B.3}$$

where

$$\Omega_i^{\cap} = \left(x_{qi}^e, x_{q(i+1)}^e\right) \tag{B.4}$$

and $\bigcup_{i=1}^{N_K-1} \overline{\Omega_i^{\cap}} = \left(\overline{\Omega} \cup \overline{\mathscr{B}\Omega} \right) \cap \mathscr{H}(x_q^e, \delta)$. Eq. (B.1) then becomes

$$D(u^{h}, v^{h}) \approx \sum_{\Omega_{e}^{h} \in \mathcal{M}^{h}} \sum_{q=1}^{N_{q}} \int_{(\Omega \cup \mathcal{B}\Omega) \cap \mathcal{H}(x_{q}^{e}, \delta)} \left[v^{h}(y) - v^{h}(x_{q}^{e}) \right] \gamma(x_{q}^{e}, y) \left[u^{h}(y) - u^{h}(x_{q}^{e}) \right] dy \omega_{q}^{e}$$

$$\approx \sum_{\Omega_{e}^{h} \in \mathcal{M}^{h}} \sum_{q=1}^{N_{q}} \sum_{\Omega_{i}^{\cap} \in \mathcal{M}^{\cap}} \int_{\Omega_{i}^{\cap}} \left[v^{h}(y) - v^{h}(x_{q}^{e}) \right] \gamma(x_{q}^{e}, y) \left[u^{h}(y) - u^{h}(x_{q}^{e}) \right] dy \omega_{q}^{e}$$
(B.5)

We now define, for $N_{qg}^{\cap} \in \mathbb{N}$, a set of Gauss quadrature points and weights to be employed for the integration over Ω_i^{\cap} as $\{x_g^{\cap}\}_{g=1}^{N_{qg}^{\cap}} \in \Omega_i^{\cap}$ and $\{\omega_g^{\cap}\}_{g=1}^{N_{qg}^{\cap}}$, respectively. Fig. B.22 shows a visual representation of the outer and inner quadrature points employed in this approach.

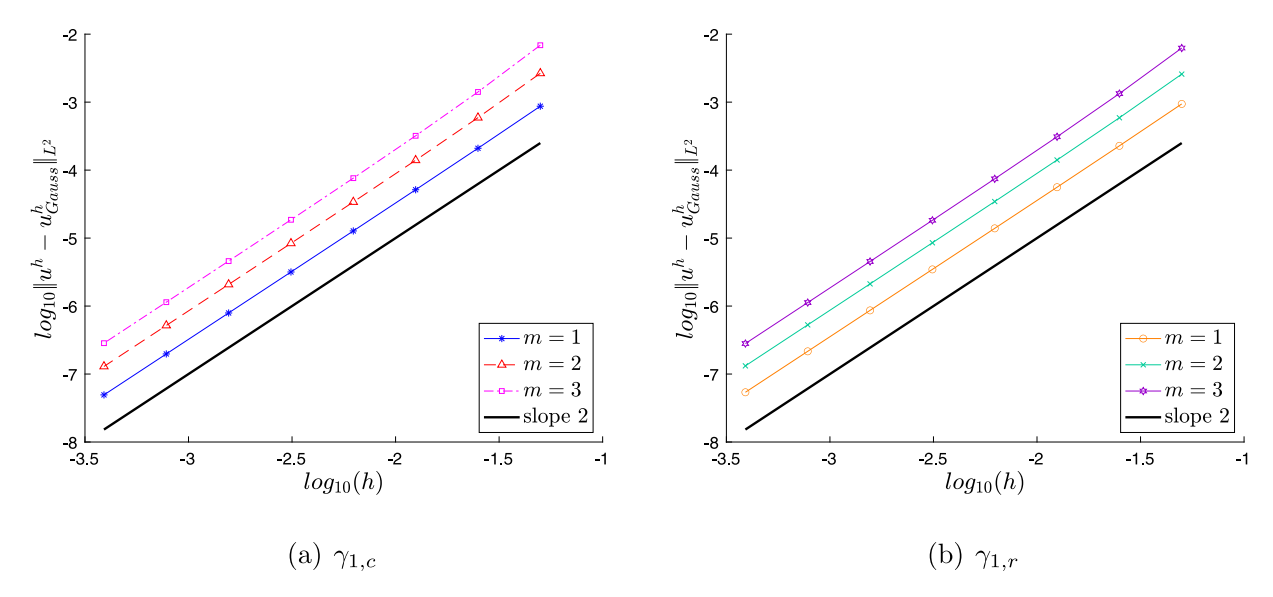


Fig. B.23. L^2 norm convergence behaviors of the difference between the one-dimensional numerical solution obtained with the optimization-based approach and the solution obtained with inner Gauss quadrature over elements-ball intersections, for the case with exact local sinusoidal solution. m = 1, 2, 3, uniform discretization, and $t_e = \delta$. $N_q = 40$, $\overline{N}_{qp} = 10$, and $N_{qg}^0 = 10$ are employed. $\gamma_{1,c}$ and $\gamma_{1,r}$ are both considered.

Now, Eq. (B.5) becomes

$$D(u^{h}, v^{h}) \approx \sum_{\Omega_{e}^{h} \in \mathcal{M}^{h}} \sum_{q=1}^{N_{q}} \int_{(\Omega \cup \mathcal{B}\Omega) \cap \mathcal{H}(x_{q}^{e}, \delta)} \left[v^{h}(y) - v^{h}(x_{q}^{e}) \right] \gamma(x_{q}^{e}, y) \left[u^{h}(y) - u^{h}(x_{q}^{e}) \right] dy \omega_{q}^{e}$$

$$\approx \sum_{\Omega_{e}^{h} \in \mathcal{M}^{h}} \sum_{q=1}^{N_{q}} \sum_{\Omega_{i}^{\cap} \in \mathcal{M}^{\cap}} \int_{\Omega_{i}^{\cap}} \left[v^{h}(y) - v^{h}(x_{q}^{e}) \right] \gamma(x_{q}^{e}, y) \left[u^{h}(y) - u^{h}(x_{q}^{e}) \right] dy \omega_{q}^{e}$$

$$\approx \sum_{\Omega_{e}^{h} \in \mathcal{M}^{h}} \sum_{q=1}^{N_{q}} \sum_{\Omega \cap \mathcal{M}^{\cap}} \sum_{q=1}^{N_{qg}^{\cap}} \left[v^{h}(x_{q}^{\cap}) - v^{h}(x_{q}^{e}) \right] \gamma(x_{q}^{e}, x_{q}^{\cap}) \left[u^{h}(x_{q}^{\cap}) - u^{h}(x_{q}^{e}) \right] \omega_{qg}^{\cap} \omega_{q}^{e}.$$
(B.6)

We then solve the one-dimensional problem with exact local sinusoidal solution and uniform discretization (see Section 6.1.1) and compare in Fig. B.23 the results $u_{Gauss}^h(x)$ obtained with this approach (e.g., by using Eq. (B.6)) with the results obtained with the optimization-based quadrature approach presented in Sections 3 and 4, $u^h(x)$. Fig. B.23 shows the L^2 norm convergence behavior of the difference between the two solutions as h is refined, computed by replacing u_0 with u_{Gauss}^h in Eq. (92) for $N_{gs} = 8$. We note that attempting to refine the sinusoidal case further, the error becomes dominated by floating point arithmetic. However, we observe that the difference between the two considered schemes decreases with a second-order rate as h is refined. Since we showed in Section 6.1 that the optimization-based quadrature approach shows second-order convergence to the exact local solution, and linear FEM is a second-order method, the difference between the two approaches here compared is expected to be at least second-order convergent via triangle inequality. The obtained results are consistent with this and suggest that the second-order bound is strict.

References

- [1] D. Benson, S. Wheatcraft, M. Meerschaert, Application of a fractional advection-dispersion equation, Water Resour. Res. 36 (6) (2000) 1403–1412.
- [2] D. Benson, R. Schumer, M. Meerschaert, S. Wheatcraft, Fractional dispersion, Lévy motion, and the MADE tracer tests, Transp. Porous Media 42 (2001) 211–240.
- [3] M. D'Elia, M. Gulian, Analysis of anisotropic nonlocal diffusion models: Well-posedness of fractional problems for anomalous transport, Numer. Math.: Theory Methods Appl. (2021) Accepted.

- [4] Z.-Q. Deng, V. Singh, L. Bengtsson, Numerical solution of fractional advection-dispersion equation, J. Hydraul. Eng. 130 (5) (2004).
- [5] R. Schumer, D. Benson, M. Meerschaert, B. Baeumer, Multiscaling fractional advection-dispersion equations and their solutions, Water Resour. Res. 39 (1) (2003) 1022–1032.
- [6] R. Schumer, D. Benson, M. Meerschaert, S. Wheatcraft, Eulerian derivation of the fractional advection-dispersion equation, J. Contam. Hydrol. 48 (2001) 69–88.
- [7] Y.D. Ha, F. Bobaru, Characteristics of dynamic brittle fracture captured with peridynamics, Eng. Fract. Mech. 78 (6) (2011) 1156–1168.
- [8] D. Littlewood, Simulation of dynamic fracture using peridynamics, finite element modeling, and contact, in: Proceedings of the ASME 2010 International Mechanical Engineering Congress and Exposition, Vancouver, British Columbia, Canada, Vol. 9, 2010, pp. 209–217.
- [9] S. Silling, Reformulation of elasticity theory for discontinuities and long-range forces, J. Mech. Phys. Solids 48 (2000) 175–209.
- [10] A. Akhavan-Safaei, M. Samiee, M. Zayernouri, Data-driven fractional subgrid-scale modeling for scalar turbulence: A nonlocal LES approach, J. Comput. Phys. (2021) 110571.
- [11] P.C.D. Leoni, T.A. Zaki, G. Karniadakis, C. Meneveau, Two-point stress-strain rate correlation structure and non-local eddy viscosity in turbulent flows, J. Fluid Mech. 914 (2021) A6.
- [12] G. Pang, M. D'Elia, M. Parks, G.E. Karniadakis, nPINNs: nonlocal physics-informed neural networks for a parametrized nonlocal universal Laplacian operator. Algorithms and applications, J. Comput. Phys. 422 (2020) 109760.
- [13] A. Buades, B. Coll, J. Morel, Image denoising methods. A new nonlocal principle, SIAM Rev. 52 (2010) 113-147.
- [14] M. D'Elia, J.C. De Los Reyes, A. Miniguano-Trujillo, Bilevel parameter learning for nonlocal image denoising models, J. Math. Imaging Vision 63 (6) (2021) 753–775.
- [15] G. Gilboa, S. Osher, Nonlocal linear image regularization and supervised segmentation, Multiscale Model. Simul. 6 (2007) 595-630.
- [16] N. Burch, M. D'Elia, R. Lehoucq, The exit-time problem for a Markov jump process, Eur. Phys. J. Spec. Top. 223 (2014) 3257-3271.
- [17] M. D'Elia, Q. Du, M. Gunzburger, R. Lehoucq, Nonlocal convection-diffusion problems on bounded domains and finite-range jump processes, Comput. Methods Appl. Math. 29 (2017) 71–103.
- [18] M. Meerschaert, A. Sikorskii, Stochastic Models for Fractional Calculus, Studies in Mathematics, Gruyter, 2012.
- [19] R. Metzler, J. Klafter, The random walk's guide to anomalous diffusion: A fractional dynamics approach, Phys. Rep. 339 (2000) 1–77.
- [20] R. Metzler, J. Klafter, The restaurant at the end of the random walk: recent developments in the description of anomalous transport by fractional dynamics, J. Phys. A 37 (2004) 161–208.
- [21] M. D'Elia, M. Gulian, H. Olson, G.E. Karniadakis, Towards a unified theory of fractional and nonlocal vector calculus, Fract. Calc. Appl. Anal. 24 (5) (2021) 1301–1355.
- [22] G. Capodaglio, M. D'Elia, P. Bochev, M. Gunzburger, An energy-based coupling approach to nonlocal interface problems, Comput. & Fluids 207 (2020) 104593.
- [23] X. Xu, C. Glusa, M. D'Elia, J.T. Foster, A FETI approach to domain decomposition for meshfree discretizations of nonlocal problems, Comput. Methods Appl. Mech. Engrg. (2021, accepted).
- [24] X. Xu, M. D'Elia, J.T. Foster, A machine-learning framework for peridynamic material models with physical constraints, Comput. Methods Appl. Mech. Engrg. (2021, accepted).
- [25] O. Burkovska, C. Glusa, M. D'Elia, An optimization-based approach to parameter learning for fractional type nonlocal models, Comput. Math. Appl. (2021).
- [26] M. D'Elia, M. Gunzburger, Optimal distributed control of nonlocal steady diffusion problems, SIAM J. Control Optim. 55 (2014) 667–696.
- [27] M. D'Elia, M. Gunzburger, Identification of the diffusion parameter in nonlocal steady diffusion problems, Appl. Math. Optim. 73 (2016) 227–249.
- [28] M. Gulian, M. Raissi, P. Perdikaris, G.E. Karniadakis, Machine learning of space-fractional differential equations, SIAM J. Sci. Comput. 41 (4) (2019) A2485–A2509.
- [29] G. Pang, L. Lu, G.E. Karniadakis, fPINNs: Fractional physics-informed neural networks, SIAM J. Sci. Comput. 41 (2019) A2603–A2626.
- [30] G. Pang, P. Perdikaris, W. Cai, G.E. Karniadakis, Discovering variable fractional orders of advection-dispersion equations from field data using multi-fidelity Bayesian optimization, J. Comput. Phys. 348 (2017) 694–714.
- [31] X. Xu, M. D'Elia, J.T. Foster, A machine-learning framework for peridynamic material models with physical constraints, Comput. Methods Appl. Mech. Engrg. 386 (2021) 114062.
- [32] H. You, Y. Yu, N. Trask, M. Gulian, M. D'Elia, Data-driven learning of nonlocal physics from high-fidelity synthetic data, Comput. Methods Appl. Mech. Engrg. 374 (2021) 113553.
- [33] H. You, Y. Yu, S. Silling, M. D'Elia, Data-driven learning of nonlocal models: from high-fidelity simulations to constitutive laws, 2020, Accepted in AAAI MLPS Symposium.
- [34] H. You, Y. Yu, S. Silling, M. D'Elia, A data-driven peridynamic continuum model for upscaling molecular dynamics, Comput. Methods Appl. Mech. Engrg. (2021, accepted).
- [35] M. Ainsworth, C. Glusa, Towards an efficient finite element method for the integral fractional Laplacian on polygonal domains, in: Contemporary Computational Mathematics-a Celebration of the 80th Birthday of Ian Sloan, Springer, 2018, pp. 17–57.
- [36] G. Capodaglio, M. D'Elia, M. Gunzburger, P. Bochev, M. Klar, C. Vollmann, A general framework for substructuring-based domain decomposition methods for models having nonlocal interactions, Numer. Methods Partial Differential Equations (2020).
- [37] M. D'Elia, Q. Du, C. Glusa, X. Tian, Z. Zhou, Numerical methods for nonlocal and fractional models, ACTA Numer. 29 (2020).
- [38] M. D'Elia, M. Gunzburger, C. Vollmann, A cookbook for approximating euclidean balls and for quadrature rules in finite element methods for nonlocal problems, Math. Models Methods Appl. Sci. 31 (08) (2021) 1505–1567.
- [39] M. Pasetto, Enhanced Meshfree Methods for Numerical Solution of Local and Nonlocal Theories of Solid Mechanics, (Ph.D. thesis), University of California, San Diego, CA, 2019.

- [40] M. Pasetto, Y. Leng, J. Chen, J. Foster, P. Seleson, A reproducing kernel enhanced approach for peridynamic solutions, Comput. Methods Appl. Mech. Engrg. 340 (2018) 1044–1078.
- [41] S.A. Silling, E. Askari, A meshfree method based on the peridynamic model of solid mechanics, Comput. Struct. 83 (17–18) (2005) 1526–1535.
- [42] H. Wang, K. Wang, T. Sircar, A direct O(N log²N) finite difference method for fractional diffusion equations, J. Comput. Phys. 229 (21) (2010) 8095–8104.
- [43] Y. Chen, J. Lee, A. Eskandarian, Meshless Methods in Solid Mechanics, Springer Science & Business Media, 2006.
- [44] M. Parks, D. Littlewood, J. Mitchell, S. Silling, Peridigm Users Guide, Technical Report SAND2012-7800, Sandia National Laboratories, NM, USA, 2012.
- [45] M. Parks, P. Seleson, S. Plimpton, R. Lehoucq, S. Silling, Peridynamics with LAMMPS:A User Guide, Technical Report SAND2010-5549, Sandia National Laboratories, NM, USA, 2010.
- [46] N. Trask, H. You, Y. Yu, M.L. Parks, An asymptotically compatible meshfree quadrature rule for nonlocal problems with applications to peridynamics, Comput. Methods Appl. Mech. Engrg. 343 (2019) 151–165.
- [47] M. Gunzburger, R. Lehoucq, A nonlocal vector calculus with application to nonlocal boundary value problems, Multiscale Model. Simul. 8 (2010) 1581–1598.
- [48] Q. Du, M. Gunzburger, R. Lehoucq, K. Zhou, A nonlocal vector calculus, nonlocal volume constrained problems, and nonlocal balance laws, Math. Models Appl. Sci. 23 (3) (2013) 493–540.
- [49] E. Aulisa, G. Capodaglio, A. Chierici, M. D'Elia, Efficient quadrature rules for finite element discretizations of nonlocal equations, Numer. Methods Partial Differential Equations (2021).
- [50] Y. Leng, X. Tian, N. Trask, J. Foster, Asymptotically compatible reproducing kernel collocation and meshfree integration for nonlocal diffusion, SIAM J. Numer. Anal. 59 (2021) 88–118.
- [51] B. Gross, N. Trask, P. Kuberry, P. Atzberger, Meshfree methods on manifolds for hydrodynamic flows on curved surfaces: A generalized moving least-squares (GMLS) approach, J. Comput. Phys. 409 (2020) 109–340.
- [52] M. D'Elia, Q. Du, M. Gunzburger, R. Lehoucq, Nonlocal convection-diffusion problems on bounded domains and finite-range jump processes, Comput. Methods Appl. Math. 17 (4) (2017) 707–722.
- [53] M. Felsinger, M. Kassmann, P. Voigt, The Dirichlet problem for nonlocal operators, Math. Z. 279 (3-4) (2015) 779-809.
- [54] T. Mengesha, Q. Du, Analysis of a scalar nonlocal peridynamic model with a sign changing kernel, Discrete Contin. Dyn. Syst. Ser. B 18 (5) (2013) 1415.
- [55] Q. Du, M. Gunzburger, R. Lehoucq, K. Zhou, Analysis and approximation of nonlocal diffusion problems with volume constraints, SIAM Rev. 54 (4) (2012) 667–696.
- [56] M. Gunzburger, R. Lehoucq, A nonlocal vector calculus with applications to nonlocal boundary value problems, Multiscale Model. Simul. 8 (5) (2010) 1581–1598.
- [57] M. D'Elia, X. Tian, Y. Yu, A physically-consistent, flexible and efficient strategy to convert local boundary conditions into nonlocal volume constraints, SIAM J. Sci. Comput. 42 (4) (2020) A1935–A1949.
- [58] M. D'Elia, Y. Yu, On the prescription of boundary conditions for nonlocal Poisson's and peridynamics models, 2021, arXiv preprint arXiv:2107.04450.
- [59] D. Mirzaei, R. Schaback, M. Dehghan, On generalized moving least squares and diffuse derivatives, IMA J. Numer. Anal. 32 (2012) 983–1000
- [60] R. Salehi, M. Dehghan, A generalized moving least square reproducing kernel method, J. Comput. Appl. Math. 249 (2013) 120-132.
- [61] D. Mirzaei, R. Schaback, Direct meshless local Petrov-Galerkin (DMLPG) method: A generalized MLS approximation, Appl. Numer. Math. 68 (2013) 73–82.
- [62] J. Chen, M. Hillman, S.-W. Chi, Meshfree methods: Progress made after 20 years, J. Eng. Mech. 143 (4) (2017).
- [63] Q. Du, M. Gunzburger, R. Lehoucq, K. Zhou, Analysis and approximation of nonlocal diffusion problems with volume constraints, SIAM Rev. 54 (2012) 667–696.
- [64] X. Tian, Q. Du, Asymptotically compatible schemes and applications to robust discretizations of nonlocal models, SIAM J. Numer. Anal. 52 (4) (2014) 1641–1665.
- [65] F. Bobaru, J. Foster, P. Geubelle, S. Silling, Handbook of Peridynamic Modeling, CRC Press, 2017.
- [66] J. Bourgain, H. Brezis, P. Mironescu, Another look at Sobolev spaces, in: Optimal Control and Partial Differential Equation. Conference, Paris , FRANCE (04/12/2000), IOS Press, Amsterdam, 2001, pp. 439–455.